

Electric Potential and Field Calculation of HVDC Composite Insulators by Charge  
Simulation Method

by

Jiahong He

A Thesis Presented in Partial Fulfillment  
of the Requirements for the Degree  
Master of Science

Approved November 2013 by the  
Graduate Supervisory Committee:

Ravi Gorur, Chair  
Raja Ayyanar  
Keith Holbert

ARIZONA STATE UNIVERSITY

December 2013

## ABSTRACT

High Voltage Direct Current (HVDC) technology is being considered for several long distance point-to-point overhead transmission lines, because of their lower losses and higher transmission capability, when compared to AC systems. Insulators are used to support and isolate the conductors mechanically and electrically. Composite insulators are gaining popularity for both AC and DC lines, for the reasons of light weight and good performance under contaminated conditions.

This research illustrates the electric potential and field computation on HVDC composite insulators by using the charge simulation method. The electric field is calculated under both dry and wet conditions. Under dry conditions, the field distributions along the insulators whose voltage levels range from 500 kV to 1200 kV are calculated and compared. The results indicate that the HVDC insulator produces higher electric field, when compared to AC insulator. Under wet conditions, a 500 kV insulator is modeled with discrete water droplets on the surface. In this case, the field distribution is affected by surface resistivity and separations between droplets. The corona effects on insulators are analyzed for both dry and wet conditions. Corona discharge is created, when electric field strength exceeds the threshold value. Corona and grading rings are placed near the end-fittings of the insulators to reduce occurrence of corona. The dimensions of these rings, specifically their radius, tube thickness and projection from

end fittings are optimized. This will help the utilities design proper corona and grading rings to reduce the corona phenomena.

## ACKNOWLEDGMENTS

First of all, I would like to express my sincere gratitude to Professor Ravi S. Gorur for his continuous guidance and support in my two years study. His advice, patience and understanding not only help me with my academic research but also improve my communication skills and career development.

I especially want to thank Professor Raja Ayyanar and Professor Keith Holbert. Thank you for your time and consideration to be my committee members.

In addition, I am also grateful for all the professors in the power system group. In my two years study, I have learned a lot from each course.

I would like to acknowledge all my friends at Arizona State University, who encourage me and give me confidence as always.

Finally, I would like to thank my parents for their extended care and support.

## TABLE OF CONTENT

CHAPTER	PAGE
LIST OF TABLES.....	vii
LIST OF FIGURES .....	viii
1. INTRODUCTION .....	1
1.1 Introduction to high voltage insulators.....	1
1.2 Research objectives .....	4
1.3 Organization and content.....	5
2. INSULATORS AND SIMPLIFIED MODELS .....	6
2.1 INTRODUCTION.....	6
2.2 Types of insulators.....	6
2.2.1 Porcelain insulators.....	6
2.2.2 Glass insulators .....	8
2.2.3 Composite insulators.....	9
2.3 Property comparison of AC and DC insulators .....	12
2.3.1 Simplified insulator model with AC supply .....	12
2.3.2 Simplified insulator model with DC supply .....	13
3. ELECTRIC FIELD COMPUTATION TECHENIQIES .....	14
3.1 Introduction.....	14
3.2 Experimental methods.....	16

CHAPTER	PAGE
3.3 Analytical field computation methods .....	16
3.4 Numerical field computation methods.....	17
3.4.1 Finite difference method .....	17
3.4.2 Finite element method.....	19
3.4.3 Boundary element method .....	22
3.4.4 Charge simulation method .....	23
4. CHARGE SIMULATION METHOD AND EQUATIONS.....	25
4.1 INTRODUCTION.....	25
4.2 SIMULATING MODEL DIMENSIONS .....	25
4.2.1 INSULATOR GEOMETRY UNDER DRY SURFACE CONDITION	25
4.2.2 INSULATOR GEOMETRY UNDER WET SURFACE CONDITION	27
4.3 BOUNDARY CONDITION AND COMPUTATION METHOD .....	28
4.3.1 GOVERNING EQUATIONS UNDER DRY SURFACE CONDITIONS	28
.....	28
4.3.2 GOVERNING EQUATIONS UNDER WET SURFACE CONDITIONS	30
.....	30
5. ELECTRIC POTENTIAL AND FIELD ANALYSIS .....	34
5.1 Introduction.....	34
5.2 Simulating results under dry conditions .....	34

CHAPTER	PAGE
5.2.1 HVAC insulators.....	34
5.2.2 HVDC insulators.....	37
5.2.3 Comparison between HVDC and HVAC insulators.....	41
5.3 Simulating results under wet conditions .....	42
5.3.1 HVAC insulators.....	43
5.3.2 HVDC insulators.....	44
5.3.3 Effects of space between water droplets .....	45
6. OPTIMIZATION OF GRADING RINGS .....	48
6.1 Introduction.....	48
6.2 Grading ring optimization under dry conditions .....	49
6.2.1 Optimization for HVAC insulators .....	49
6.2.2 Optimization for HVDC insulators.....	54
6.3 Grading ring optimization under wet conditions .....	61
6.3.1 Optimization for HVAC insulators.....	61
6.3.2 Optimization for HVDC insulators.....	64
7. CONCLUSIONS AND FUTURE WORK.....	67
7.1 Conclusions.....	67
7.2 Future works .....	68
REFERENCES .....	69

## LIST OF TABLES

TABLE	PAGE
1 The dimension for AC composite insulators .....	34
2 The dimension for DC composite insulators .....	39
3 Arrangement of water droplets with AC voltage supply .....	43
4 Arrangement of water droplets with DC voltage supply .....	44
5 Four cases of different gaps between water droplets.....	45

## LIST OF FIGURES

FIGURE	PAGE
1. The cap-and-pin insulator .....	6
2. The long rod suspension insulator .....	7
3. The suspension glass insulators [4] .....	9
4. The composite suspension insulator .....	10
5. Line post suspension insulator.....	10
6. Insulator model with AC supply.....	12
7. Insulator model with DC supply.....	13
8. FEM field division and example triangle element $ijm$ .....	20
9. Schematic of the insulator model .....	25
10. Charges and contour points in the electrode.....	26
11. Simulated charges and contour points arrangements in the insulator .....	26
12. Water droplets on the insulator surface .....	27
13. Contour points and charges arrangements in one water droplet.....	27
14. Normal flux density vector of water droplets.....	32
15. Potential distribution along HVAC insulator surfaces under dry conditions. ....	35
16. Electric field distribution along HVAC insulator surfaces under dry conditions. ....	36
17. Normalized positive and negative DC potential distribution .....	37
18. Normalized positive and negative DC electric field distribution .....	38

19. Potential distribution along HVDC insulator surfaces under dry conditions. .... 39

FIGURE PAGE

20. Electric field distribution along HVDC insulator surfaces under dry conditions. 40

21. Normalized AC and DC potential distribution..... 41

22. Normalized AC and DC electric field distribution..... 42

23. Electric field distribution along HVAC insulator surfaces under wet conditions. 43

24. Electric field distribution with water droplets and +500 kV DC voltage..... 44

25. Electric field distribution with water droplets and -500 kV DC voltage..... 45

26. Electric field distribution with different spaces between water droplets. .... 46

27. The maximum electric field distributions as a function of spaces between water droplets ..... 47

28. Cross section schematic of rod insulator model with corona and grading rings... 48

29. Impact of grading ring radius on field distribution with AC voltage supply ..... 49

30. Maximum electric field as a function of ring radius of the HVAC insulator..... 50

31. Impact of grading ring tube thickness on field distribution with AC voltage supply. .... 51

32. Maximum electric field as a function of tube thickness of the HVAC insulator .. 51

33. Impact of projection from the end-fitting on field distribution with AC voltage supply ..... 52

34. Maximum electric field as a function of projection of the HVAC insulator..... 53

35. Electric field distribution along HVAC insulator surfaces with optimized corona and grading rings .....	54
---	----

FIGURE	PAGE
36. Electric field distribution along the insulator surface with HVAC corona and grading rings under -500 kV voltage supply .....	55
37. Impact of grading ring radius on field distribution with DC voltage supply .....	56
38. Maximum electric field as a function of radius of the HVDC insulator .....	57
39. Impact of tube thickness on field distribution with DC voltage supply .....	58
40. Maximum electric field as a function of tube thickness of the HVDC insulator ..	58
41. Impact of projection from end fitting on field distribution with DC voltage supply	59
42. Maximum electric field as a function of projections from the end fitting.....	60
43. Electric field distribution along HVDC insulator surfaces with optimized corona and grading rings .....	60
44. Maximum electric field as a function of ring radius of the HVAC insulator.....	61
45. Maximum electric field as a function of ring tube thicknesses of the HVAC insulator .....	62
46. Maximum electric field as a function of projections from the end-fitting .....	62
47. Electric field distribution of HVAC insulator surfaces with optimized corona and grading rings .....	63
48. Maximum electric field as a function of radius of the HVDC insulator .....	64

49. Maximum electric field as a function of tube thicknesses of the HVDC insulator 65

50. Maximum electric field as a function of projections of the HVDC insulator ..... 65

FIGURE	PAGE
51. Electric field distribution of HVDC insulator surfaces with optimized corona and grading rings.....	66

## NOMENCLATURE

AC	Alternating current
B	Magnetic flux density
BEM	Boundary element method
CSM	Charge simulation method
D	Electric flux density
DC	Direct Current
E	Electric field intensity
EHV	Extra High Voltage
FEM	Finite Element Method
HVAC	High Voltage Alternating Current
HVDC	High Voltage Direct Current
IEEE	Institute of Electrical and Electronics Engineers
kV	Kilo Volts
P	Potential coefficient matrix
PC	Personal computer
Q	Fictitious Charge matrix
UHV	Ultra High Voltage
V	Voltage matrix on contour points

# 1. INTRODUCTION

## 1.1 Introduction to high voltage insulators

High voltage transmission lines bring power from remote generating stations to consumers. HVDC technology is being considered for several long distance transmission lines, because of their lower losses and higher transmission capability, when compared to AC systems [1].

The first transmission line was a DC transmission line built in 1882 at Miesbach-Munich Power Transmission. The technologies of inverters and converters were not fully developed at that time. Hence, the voltage level of DC transmission systems could not reach high enough values to reduce the losses during long distance transmission. Meanwhile, the AC voltage was easily increased by transformers. Therefore, the losses and capital cost of AC transmission systems were lower than that of DC systems, and the DC transmission was then replaced by AC in 1886. However, HVDC technology has risen and gained popularity during recent years, thanks to fast development of power electronic devices. The United States of America, Canada, Russia and several other countries have built and operated HVDC systems for decades [1]. China completed a HVDC transmission system at  $\pm 800$  kV in 2009 [2]. The advantages of HVDC system are listed as follows [3]:

1) When compared to AC system, transmission loss of HVDC system is reduced by approximately 1/3 and the transmission capacity is dramatically increased, due to low resistance and reduced reactive power loss.

2) The DC transmission lines can connect two large scale grids, which can be unsynchronized, or they can be at different frequencies. The fault propagation from one grid to another can be prevented by HVDC connection.

3) The capital cost of HVDC system construction is less than that of AC system for the long distance power transmission. Even though the conversion stations of HVDC system at the terminals are expensive, the cost of HVDC conductors are significantly less, due to reduced number of conductors and thinner conductors.

Insulators are used to provide mechanical support of transmission lines as well as electrically isolate the conductors from ground. Composite insulators are gaining popularity for both AC and DC lines, for the reasons of light weight and good performance under contaminated conditions. Composite insulator design must consider all operating conditions, such as surges, contamination, weathering, etc. Electric field along composite insulators is dependent on both surface and volume properties [2]. The volume properties are affected by internal defects in the insulators. The external factors such as rain, mist and ice dramatically reduce the surface resistance and intensify the field strength.

Corona discharge is caused by the ionization of the air surrounding the lines and insulators, when electric field strength exceeds a corona threshold of 15.2 kV/cm (dry surface) or 4 kV/cm (wet surface). This phenomenon could lead to energy loss, radio interference and insulator lifetime reduction [4]. In order to reduce corona occurrence, corona and grading rings are placed near the end-fittings of the insulator. The field distribution is affected by three main factors of grading rings dimensions: ring radius, tube thickness and the projection from end-fittings.

Since mitigation of electric field strength along the insulator surface is the key to reduce the corona phenomena, many methods are used to measure and calculate the electric field distribution. These methods can be categorized into two classes: laboratory experiments and computer simulations. Since laboratory experiments are time-consuming and costly, simulations are conducted first to optimize the insulator design. Laboratory experiments are then conducted to verify the simulation results. With development of computer technology, numerical methods are employed in electric potential and field simulation. The common numerical methods are finite element method (FEM), finite difference method (FDM), method of moments, boundary element method (BEM), Monte Carlo method, and charge simulation method (CSM) [5]. It has been shown that for insulators that are rotationally symmetric, the CSM has certain advantages in terms of computational complexity [6]. Therefore, CSM is utilized to analyze the HVDC insulator properties in this thesis.

## 1.2 Research objectives

This work focuses on the electric potential and field computation along the insulator surface by using charge simulation method. The aim is to determine suitable dimensions of the insulators under dry and wet conditions with AC and DC voltage supply. The voltage levels range from 500 kV to 1200 kV. The research objectives are listed as follows:

- Optimize charge simulation method to get accurate results.
- Calculate the electric potential and field distribution of dry insulators at AC to provide reference for comparison.
- Calculate the electric potential and field distribution of dry insulators at DC and compare the results with AC.
- Calculate the electric potential and field distribution of wet insulators at AC to provide reference for comparison.
- Calculate the electric potential and field distribution of wet insulators at DC and compare the results with AC.
- Optimize grading and corona ring dimensions.

### **1.3 Organization and content**

This thesis is divided into seven chapters.

Chapter 1 discusses the development history of HVDC and HVAC transmission, and shows the advantages of HVDC transmission systems.

Chapter 2 introduces three types of insulators in high voltage systems and gives the simplified models of HVDC and HVAC insulators.

Chapter 3 briefly describes four numerical methods and comparisons are made to find the advantages of charge simulation method in the insulator simulation.

Chapter 4 gives the detailed equations of charge simulation method in dry and wet conditions with AC and DC voltage supply.

Chapter 5 illustrates the results from the simulations, conducted under wet (water droplets), and ideal (dry) conditions with DC voltage supply. These two conditions with AC voltage supply are then calculated to provide reference values.

Chapter 6 presents the electric field distributions with and without corona and grading rings, and shows the optimization of the grading rings to suppress corona.

Chapter 7 summarizes the conclusions of the present work and identifies few topics for future research.

## 2. INSULATORS AND SIMPLIFIED MODELS

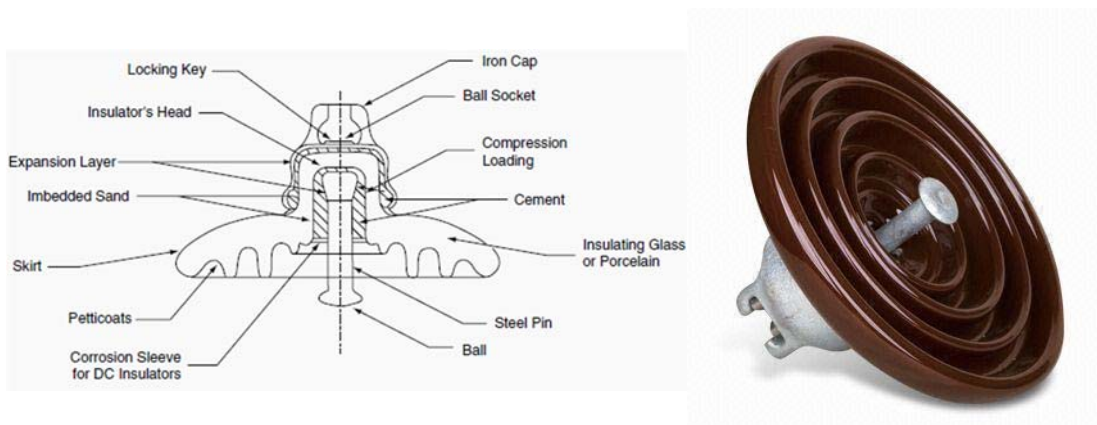
### 2.1 INTRODUCTION

Outdoor insulators are used to provide mechanical support of transmission lines and to electrically isolate the conductors from structures. Outdoor insulators are classified into three types: porcelain, glass and composite, due to different dielectric materials. In this chapter, three types of insulators are introduced in Section 2.2. The electrical models of HVAC and HVDC insulators are compared in Section 2.3.

### 2.2 Types of insulators

#### 2.2.1 Porcelain insulators

Porcelain insulators are also referred to ceramic insulators, and they have been used for more than a century [7]. These insulators can be categorized as cap-and-pin insulators and long rod suspension insulators. The schematics of cap-and-pin insulators are shown in Figure 1.



(a) The structure of cap-and-pin insulator

(b) The product of cap-and-pin insulator

Figure 1. The cap-and-pin insulator

The cap-and-pin insulators are made up of galvanized malleable iron pins and caps with Portland cement mortar. These insulators are divided into two groups: non-stacking and stacking units [4]. The non-stacking insulators contain one piece of shed between one pair of electrodes, while the stacking units have multi-piece sheds between one pair of electrodes. Compared to the cap-and-pin insulators, the rod suspension insulators are designed to avoid the puncture completely. These insulators are able to stand more severe pollution, due to the increased leakage distance [4]. The plots of long rod suspension insulators are shown in Figure 2.



(a) The structure of long rod suspension insulator (b) The product of long rod suspension insulator

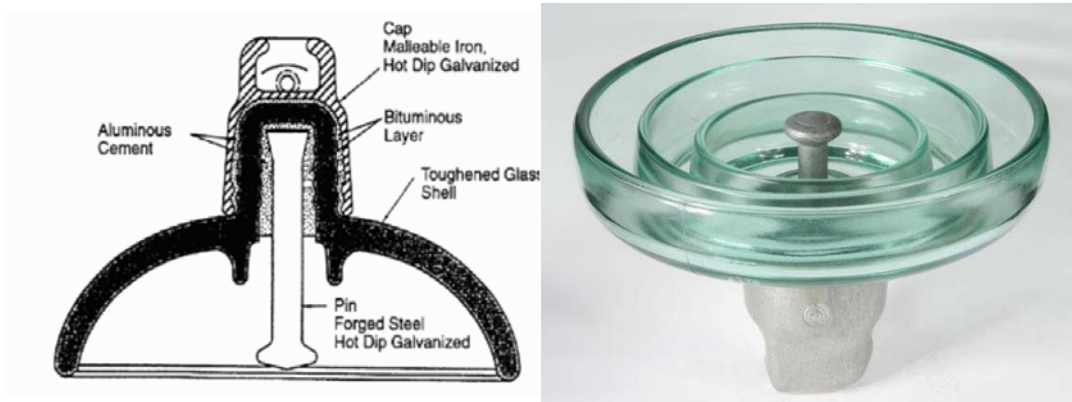
Figure 2. The long rod suspension insulator

The mechanical performances of cap-and-pin insulators and long rod suspension insulators are determined by all the components of the insulators, and require careful treatment. The electrical performance of insulators is dependent on both surface and volume properties [3]. When the porcelain insulator surfaces are wet, water tends to form a continuous film, which could lead to significant decrease of surface resistivity.

### **2.2.2 Glass insulators**

The glass is prone to fracture under stress, which increases the possibility of dropping conductors, while the cracks on the glass surface also impact the surface property and intensify the field distribution [7]. Therefore, the glass insulators did not initially provide good electrical and mechanical performance in the early ages. The materials of glass insulators have improved significantly after many experiments. Currently, the glass material is toughened by adding potassium, barium, and aluminum. The toughened insulators have a better mechanical performance than the porcelain insulators, which allow thinner shells to be used. Therefore, the voltage stress of glass insulators also increases 40%, when compared to porcelain insulators. In addition, glass insulators do not need glazing during manufacturing, and their immunity to erosion is stronger than porcelain insulators.

The glass insulators are divided into three categories, pin-type glass insulators, suspension glass insulators and multicone post insulators [4]. The most common type is suspension glass insulators. This kind of insulator is shown in Figure 3.



(a) The structure of glass insulator (b) The product of glass insulator

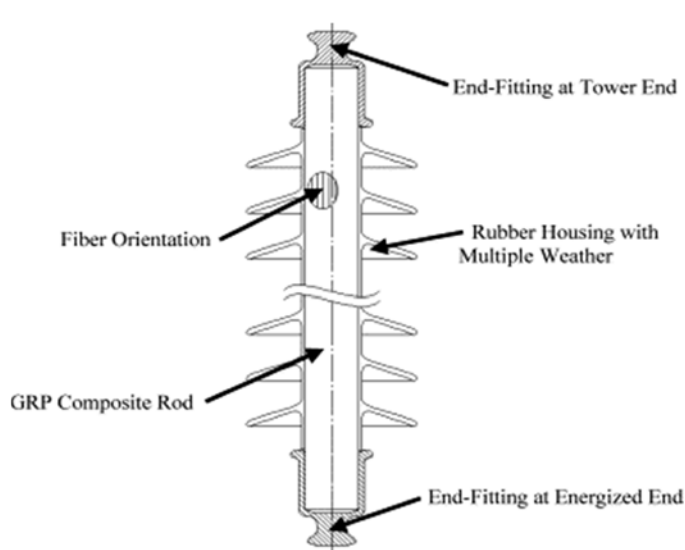
Figure 3. The suspension glass insulators [4]

### 2.2.3 Composite insulators

Composite insulators are also referred to non-ceramic insulators, whose insulation material and mechanical material are combined. The composite insulators are widely used around the world, for reasons of lighter weight and better performance under contaminated conditions. Flashover performance of composite insulators is also better than that of porcelain insulators, due to smaller diameter of the insulators and better hydrophobicity. [8].

Composite insulators are commonly made of silicone rubber and ethylene propylene rubber. Composite insulators can either be suspension type or line post type. Composite suspension insulator consists of fiberglass core, weather sheds and hardware on the end-fittings [7]. The schematics of composite suspension insulators are shown in Figure

4.

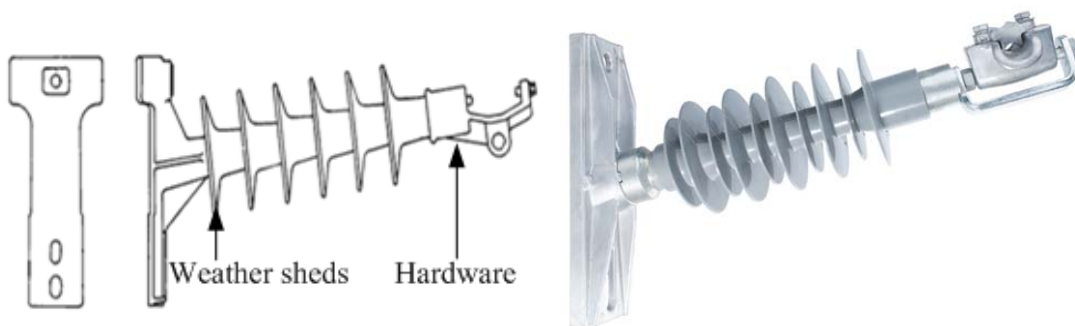


(a) The structure of suspension insulator

(b) The production of suspension insulator

Figure 4. The composite suspension insulator

Line post insulators have similar components as suspension insulators. The radius of fiber glass core of line post insulator is larger than that of suspension insulator [4], because the line post insulator needs to undertake more mechanical loads. The schematics of the line post insulators are shown below.



(a) The structure of line post insulator

(b) The production of line post insulator

Figure 5. Line post suspension insulator

Composite insulator design must consider all operating conditions, such as surges, contamination, weathering, etc. Composite insulators for DC lines can experience more problems when compared to AC lines, due to increased nonlinearity of voltage distribution, which also helps to increase the contamination on the insulator.

## 2.3 Property comparison of AC and DC insulators

### 2.3.1 Simplified insulator model with AC supply

The insulator with AC voltage is modeled as a capacitor in parallel with a resistor shown in Figure 6 [30].

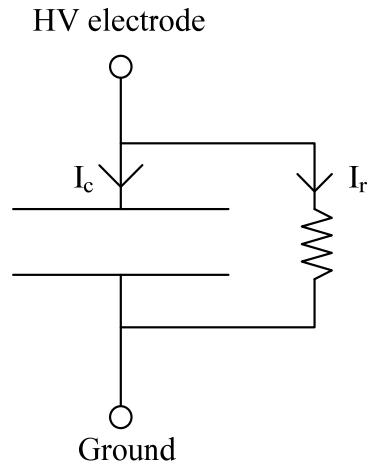


Figure 6. Insulator model with AC supply

In the model,  $I_c$  is the capacitive current due to AC frequency  $\omega$  and  $I_r$  is the current caused by wet surface resistivity. These two currents are the main factors affecting the electric field distribution.

The capacitive current  $I_c$  is the dominant current with AC voltage supply.  $I_c$  is commonly 100 times of  $I_r$  for good insulation.

Therefore, the total current  $I_t$  in the steady state,

$$I_t = I_c + I_r \quad (1)$$

### 2.3.2 Simplified insulator model with DC supply

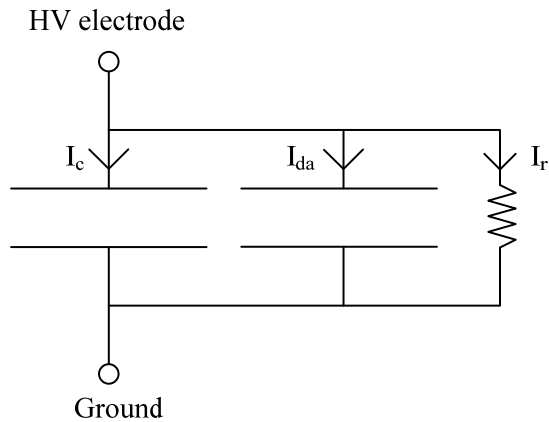


Figure 7. Insulator model with DC supply

Figure 7 shows the insulator model in DC condition. When DC voltage is applied to the insulator, the polarization realigns molecules to two poles and causes dielectric absorption current  $I_{da}$ , simulated by the extra capacitor. However,  $I_{da}$  falls to zero in several minutes, when molecules rearrangement process finishes. Like  $I_{da}$ , the capacitor injecting current  $I_c$  also reduces quickly to zero with DC voltage supply [29]. Thus, the total current in steady state is,

$$I_t = I_r \quad (2)$$

Therefore, the electric potential and field distribution is dominated by the surface resistivity and static field characteristics. In wet conditions, surface resistivity determines the field distribution. In the dry and clean condition, since the surface resistivity is large enough, the field property is close to DC static field. Therefore, the field distribution on DC insulator is more nonlinear than that on AC insulator.

### **3. ELECTRIC FIELD COMPUTATION TECHNIQUES**

#### **3.1 Introduction**

The electric potential and field distribution along the insulating surface can be affected by the factors listed below.

- 1) Voltage magnitude.
- 2) Insulating material properties.
- 3) The leakage current
- 4) Surface contamination
- 5) Internal defects

Methods that are applied to compute the electric potential and field strength along insulator surface can be divided into three classes: experimental, analytical and numerical. In this chapter, all three types of methods are introduced, and each has its own advantages and disadvantages. Among three kinds of methods, both analytical and numerical methods are simulated on the PC platform, demonstrating similar procedures: Firstly, the theoretical models based on real insulator geometry are built, and then described by integral equations or differential equations. The field details are achieved by solving those equations. In the free space, Maxwell's equations can describe all the macroscopic electromagnetic phenomena [5].

$$\left\{ \begin{array}{l} \nabla \times H = J + \frac{\partial D}{\partial t} \\ \nabla \times E = -\frac{\partial B}{\partial t} \\ \nabla \times B = 0 \\ \nabla \times D = \rho \end{array} \right. \quad (3)$$

In order to show macroscopic electromagnetic properties, three formulas are given below:

$$\left\{ \begin{array}{l} D = \varepsilon E \\ B = \mu H \\ J = \gamma E \end{array} \right. \quad (4)$$

Since the electrodes are conducting material, the principle of charge conservation is shown below.

$$\nabla \cdot J + \frac{\partial \rho}{\partial t} = 0 \quad (5)$$

Where,

$H$  = magnetic field strength

$E$  = electric field strength

$B$  = magnetic field density

$D$  = electric flux density

$J$  = current density

$\rho$  = electric charge density

$\varepsilon$  = permittivity

$\mu$  = permeability

$\gamma$  = conductivity

### **3.2 Experimental methods**

The rated voltage is energized to the sample insulators in the experimental methods. In order to get detailed results, insulators are tested under different conditions to observe the phenomena of corona and flashover. The experimental methods are the most accurate among all the methods, and the results are closest to performance of insulators in the field tests [4]. However, the experimental methods consume large amounts of time and are more costly than other methods. Therefore, the experimental methods are often used to verify the results from simulations, or to provide reference data.

### **3.3 Analytical field computation methods**

The analytical methods are to calculate the field strength directly from the original differential formulas. The results of analytical methods are precise, whereas the scale of the model that the analytical method can deal with is relatively small [10].

On one hand, the formulas are difficult to generate with complicate geometries in the practical cases, because the boundary conditions are often too uneven to be described with equations. On the other hand, as the model scale increased by the voltage level, the analytical methods require large amounts of computation resources to solve the differential equations. Therefore, the analytical methods are replaced with numerical methods.

### 3.4 Numerical field computation methods

In numerical methods, the electric field domain is described by the differential equations. The purpose of numerical methods is to transfer these equations into a linear matrix, which can be easily solved by computers. There are four steps in the process:

The first step is to transfer the field functions into a set of linear independent functions with unknown variables. The second step is to cast the continuous solution domain into a discrete form, which contains a number of elements or fictitious charges. And the third step is to minimize the error of unknown variables from linearization process. Finally, the solutions are taken into original equations to verify the results.

#### 3.4.1 Finite difference method

The principal of finite difference method is to divide the field domain with regular grid, and replace the Poisson's equations with the difference equations, whose unknown variables are the potentials at the nodes of the grid [5].

The Poisson's equations and the boundary conditions in the field D are shown below:

$$\nabla^2 u = \frac{\partial^2 u}{\partial x^2} + \frac{\partial^2 u}{\partial y^2} = F(x, y) \text{ in the domain} \quad (6)$$

$$u(x, y)|_{\Gamma} = g(\Gamma) \text{ on the boundary} \quad (7)$$

In order to build the linear matrix, the potentials at the nodes are described by Taylor series of adjacent nodes. The accuracy requirement is set as the second order. For

example, the coordinate of a two dimension node is  $(x, y)$  and the adjacent node is  $(x_0, y_0)$ .

The potential at  $(x, y)$  is described by Taylor series below:

$$\begin{aligned} \varphi(x, y) = & \varphi_0 + \left[ (x - x_0) \left( \frac{\partial \varphi}{\partial x} \right)_0 + (y - y_0) \left( \frac{\partial \varphi}{\partial y} \right)_0 \right] \\ & + \frac{1}{2} \left[ (x - x_0)^2 \left( \frac{\partial^2 \varphi}{\partial x^2} \right)_0 + 2(x - x_0)(y - y_0) \left( \frac{\partial^2 \varphi}{\partial x \partial y} \right)_0 + (y - y_0)^2 \left( \frac{\partial^2 \varphi}{\partial y^2} \right)_0 \right] \end{aligned} \quad (8)$$

In the equation, the subscript 0 represents  $(x_0, y_0)$  and the potential  $\varphi_0$  can be calculated by the average potential values of four adjacent nodes.

Therefore, the homogeneous functions with potential variables are built and the known potential values on the boundary nodes are set as  $V_i$ .

$$\begin{bmatrix} P_{11} & \cdots & P_{1i} \\ \vdots & \ddots & \vdots \\ P_{i1} & \cdots & P_{ii} \end{bmatrix} \begin{bmatrix} \varphi_1 \\ \vdots \\ \varphi_i \end{bmatrix} = \begin{bmatrix} V_1 \\ \vdots \\ V_i \end{bmatrix} \quad (9)$$

The principal of FDM is simple, and division of field is easy to complete. Finite difference method has great advantages in the two dimension field, when the shapes of boundaries are relatively simple. However, FDM can get complicated when the boundary shapes are uneven. Moreover, since infinite field domain is not able to be divided, this method cannot deal with open boundary conditions. \

### 3.4.2 Finite element method

In the previous session, it is shown that FDM focuses on the nodes of the grid and derives the linear homogeneous functions directly from Poisson's equations. Different from FDM, FEM divides the field domain by elements. These elements are small areas in the two dimension model and small volumes in the three dimension model. The related equations are then derived from coordination of each element. In addition, FEM can solve the second class boundary condition: the derivative of potential vectors. For a two dimension field domain:

$$\nabla^2 u = \frac{\partial^2 u}{\partial x^2} + \frac{\partial^2 u}{\partial y^2} = F(x, y) \quad \text{in the domain} \quad (10)$$

$$u(x, y)|_{\Gamma} = g_1(\Gamma) \quad \text{on the boundary} \quad (11)$$

$$\left. \frac{\partial u}{\partial n} \right|_{\Gamma} = g_2(\Gamma) \quad \text{on the boundary} \quad (12)$$

Triangle is the popular geometry of element used in FEM. The smaller the element, the more accurate the field strength. According to the steps above, the whole field domain can be described by each point potential of the elements [4]. An example of two dimension field discretization is shown in Figure 8.

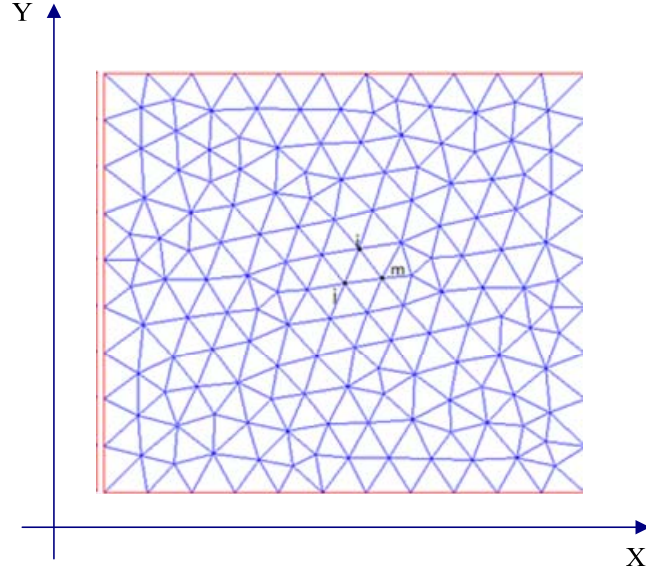


Figure 8. FEM field division and example triangle element  $ijm$

Figure 8 shows the square field domain is divided by triangle elements. The potential in each triangle has a relationship with the coordination of the triangle vertices.

$$\varphi = a_1 + a_2x + a_3y \quad (13)$$

If the discretized triangle is small enough, the field in the element is assumed as constant. Coefficients  $a_1$ ,  $a_2$  and  $a_3$  can be achieved by the equations below.

$$\begin{cases} \varphi_i = a_1 + a_2x_i + a_3y_i \\ \varphi_j = a_1 + a_2x_j + a_3y_j \\ \varphi_m = a_1 + a_2x_m + a_3y_m \end{cases} \quad (14)$$

Where  $\varphi_i$ ,  $\varphi_j$  and  $\varphi_m$  are potentials at the vertices of the triangle.

The calculated coefficients  $a_1$ ,  $a_2$  and  $a_3$  are taken back into equation:

$$\varphi = \frac{1}{2\Delta} \left[ (a_i + b_ix + c_iy)\varphi_i + (a_j + b_jx + c_jy)\varphi_j + (a_m + b_mx + c_my)\varphi_m \right] \quad (15)$$

Where  $\Delta$  is the area of the triangle  $ijm$ .

Therefore,

$$\varphi = \begin{pmatrix} N_i & N_j & N_m \end{pmatrix} \begin{pmatrix} \varphi_i \\ \varphi_j \\ \varphi_m \end{pmatrix} \quad (16)$$

Where  $N_i = (a_i + b_i x + c_i y) / 2\Delta$ ,  $N_j = (a_j + b_j x + c_j y) / 2\Delta$  and  $N_m = (a_m + b_m x + c_m y) / 2\Delta$ .

The variation problem is discretized with the principle of weighted residuals.

The matrix equation of triangle elements is shown below:

$$[K] = \begin{bmatrix} K_{ii} & K_{ij} & K_{im} \\ K_{ji} & K_{jj} & K_{jm} \\ K_{mi} & K_{mj} & K_{mm} \end{bmatrix} \quad (17)$$

In the end, the discretized linear equations are represented as,

$[K][\varphi] = [V]$ , and the unknown potentials at the vertices of all the triangles are calculated.

Designers can divide the field domain by their own purpose with FEM. For example, small elements are set in the area where electric field changes intensively to achieve accurate results; while relatively large elements are put in the area far from electrode, where field strength changes slowly to reduce the requirement of calculation resources.

However, the calculation process of FEM is more complicated than FDM and the requirement of data storage capacity is also larger. Similar to FDM, the boundary of infinite distance in FEM is difficult to deal with, as the whole field domain cannot be divided.

### 3.4.3 Boundary element method

Boundary element method focuses on the boundary conditions that affect the field domain. Unique characteristic of this method is to decrease the dimensions of the problem. For example, two dimensions problem can be described by the boundary line and reduced to one dimension problem. Three dimensions problem can be described by the boundary surface, and reduced to two dimensions problem. The procedure of boundary element method is shown below [5],

- 1) The boundary is discretized into many elements in functions with unknown potentials and normal flux densities.
- 2) The principle of weighted residuals is used to minimize the error.
- 3) The coefficient matrix is evaluated after analysis of each element.
- 4) The linear algebraic equations are then achieved with the proper boundary conditions to the nodes.
- 5) In the end, the unknown potentials can be calculated from the inversion of the coefficient matrix.

The major advantage of boundary element method is to reduce the dimensions of the space, so that the orders of the homogenous functions and the amount of input data are decreased. However, the coefficient matrix is an unsymmetrical full element matrix, which consumes large amounts of computation resources and limits the orders of the

matrix. The method makes it difficult to handle multi-media field domain, and cannot be used directly for non-linear problems.

### 3.4.4 Charge simulation method

The work presented here is based on the concept of the charge simulation method, which belongs to the category of boundary methods. This method assembles the effect of each simulating charge to calculate the electric potential and field distribution. The steps of charge simulation method are listed below [11]:

- 1) The simulating charges are introduced and set out of the field domain.
- 2) The positions of contour points are then determined on the boundaries between different media. The potentials at the contour points are known as boundary conditions.
- 3) According to the superposition principle, the equations of potentials versus simulating charges are obtained:

$$\begin{aligned}
 \varphi_1 &= P_{11}Q_1 + P_{12}Q_2 + \cdots + P_{1n}Q_n \\
 \varphi_2 &= P_{21}Q_1 + P_{22}Q_2 + \cdots + P_{2n}Q_n \\
 &\vdots \\
 \varphi_n &= P_{n1}Q_1 + P_{n2}Q_2 + \cdots + P_{nn}Q_n
 \end{aligned} \tag{18}$$

Where  $P_{ij}$  is the potential and normal flux coefficient between contour points and simulating charges,  $Q_j$  represents the unknown simulating charges and  $\varphi_i$  is the potential and normal flux on the contour points.

- 4) The equations above are solved to calculate the values of the simulating charges.

- 5) The check points are selected on the boundary to verify the accuracy requirement. If the accuracy is not satisfied, the number and positions of the simulating charges need to be rearranged.

The CSM has unique advantages over other methods in the insulator design. Firstly, CSM is suitable for three dimension field domain, especially for the symmetrical geometry (cylindrical insulator). In addition, CSM can handle the infinite field with open boundary condition. Moreover, the principle of CSM is simple and the parameters in the calculation are easily to adjust. For insulators that are rotationally symmetric, CSM can reduce the computational complexity [6, 18, 19].

Whereas, CSM requires the designers' experience to choose the right number of charges and contour points, and then place them properly to satisfy the accuracy requirement. If the coefficient matrix  $P$  gets singular, the results would have large errors.

Therefore, several means are taken to deal with the ill-condition matrix [8]:

- 1) Rearrange the positions of the contour points.
- 2) Select proper method to optimize the linear matrix. For example, the parallel complete Gaussian Pivoting Elimination Method.
- 3) Increase the digits of significant figure. For example, the double precision can be applied.

## 4. CHARGE SIMULATION METHOD AND EQUATIONS

### 4.1 INTRODUCTION

In the following section, the detailed equations of charge simulation method in multi-media are applied to analyze electric potential and field distribution of composite insulator surface. Three forms of media (electrode, insulation media and air) are categorized under dry conditions [8]; while under wet conditions, water is another medium and has different arrangements on the insulator surface [9-10].

### 4.2 SIMULATING MODEL DIMENSIONS

#### 4.2.1 INSULATOR GEOMETRY UNDER DRY SURFACE CONDITION

The insulator in this paper is modeled as a cylindrical rod with two plate electrodes. The length of the insulator varies with the dimensions of insulators. The radius of the rod model is 1 cm. Figure 9 shows the schematic of the insulator.

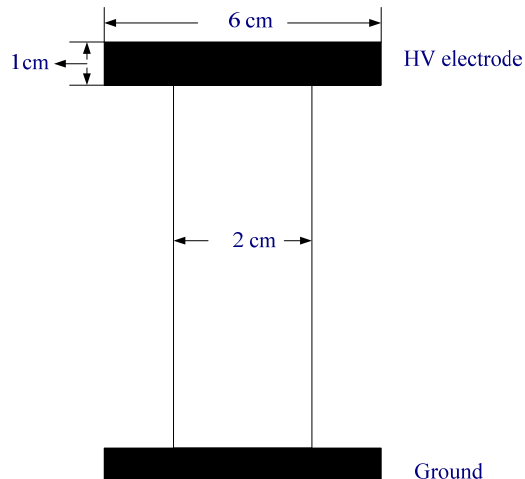


Figure 9. Schematic of the insulator model

Point charges are used in both dry and wet surface conditions, due to the unsymmetrical characteristics of water droplets.

Both electrodes have a thickness of 1 cm and radius of 3 cm. Charges and contour points arrangements in the electrode are shown in Figure 10.

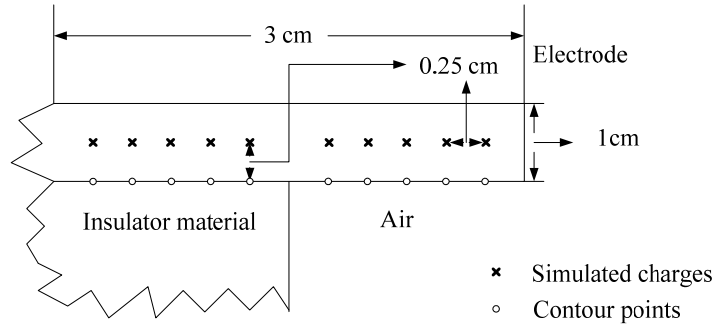


Figure 10. Charges and contour points in the electrode

Charges and contour points arrangements in the insulation material are shown in Figure 11.

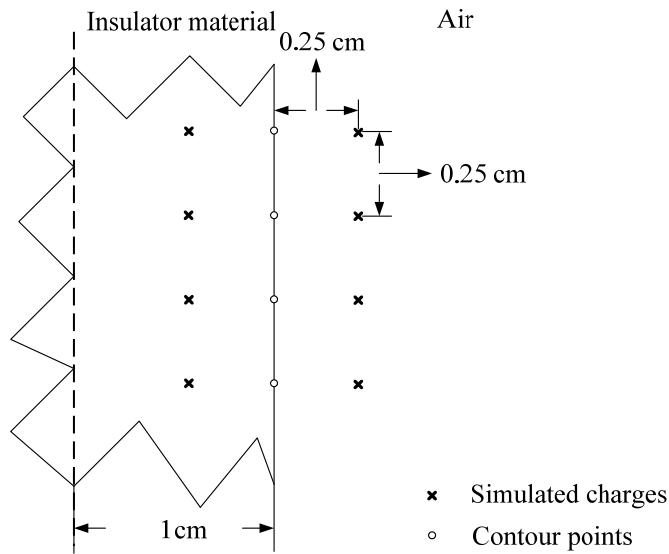


Figure 11. Simulated charges and contour points arrangements in the insulator

#### 4.2.2 INSULATOR GEOMETRY UNDER WET SURFACE CONDITION

Under wet conditions, the water droplets are modeled as spheres whose radius is 0.25 mm. The spaces between droplets are set in different values to determine the droplets impacts on electric potential and field distribution. Water droplets distribution schematic is shown in Figure 12.

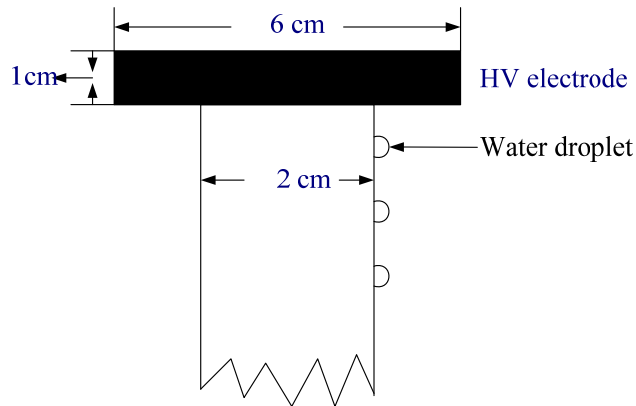


Figure 12. Water droplets on the insulator surface

Geometry of each water droplet and charges arrangement is shown in Figure 13.

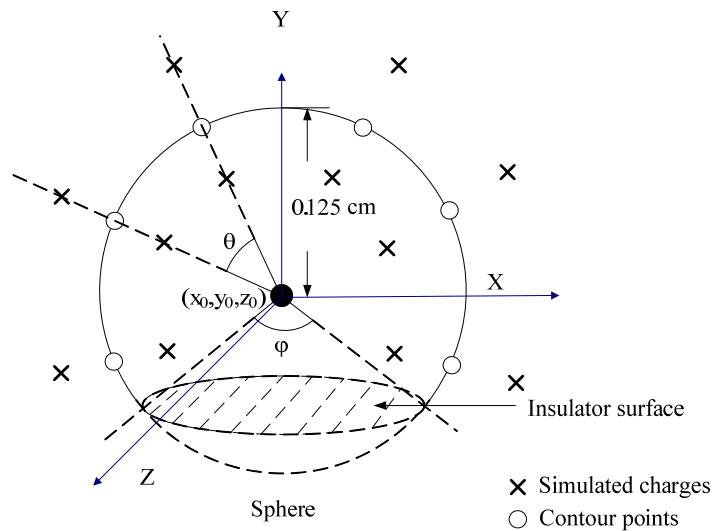


Figure 13. Contour points and charges arrangements in one water droplet

The equation in rectangular Cartesian Coordinates used to describe the sphere is:

$$\frac{(x-x_0)^2}{a^2} + \frac{(y-y_0)^2}{a^2} + \frac{(z-z_0)^2}{a^2} = 1 \quad (19)$$

Where  $a=0.5 \text{ cm}$  and  $\varphi$  is contact angle

### 4.3 BOUNDARY CONDITION AND COMPUTATION METHOD

Composite insulators under both dry and wet conditions, with AC and DC voltage supply, are simulated in this paper. Each case has different potential and flux density boundary conditions, which should be interpreted into the coefficient matrix P. The systematic equation are formulated as,

$$[P][Q]=[φ] \quad (20)$$

P is  $m \times n$  coefficient matrix, Q is  $n \times 1$  unknown simulated charges matrix, and  $\varphi$  is the potential or electric field strength at the contour points.

The number of charges in the electrode is defined as  $n_e$ , while  $n_i$ , and  $n_a$  represent the number of charges in the insulator, and in the air respectively.  $n_w$  represents all the charges in the water droplets and  $n_{sw}$  represents the number of charges in one single water droplet.

#### 4.3.1 GOVERNING EQUATIONS UNDER DRY SURFACE CONDITIONS

The potential and flux density must satisfy [11],

On the electrode and air interface,

$$\sum_{j=1}^{n_e+n_i} P_{ij} Q_j = \varphi \quad (21)$$

On the electrode and insulator interface,

$$\sum_{j=1}^{n_e+n_a} P_{ij} Q_j = \varphi \quad (22)$$

On the insulator and air interface

$$\begin{aligned} \sum_{j=1}^{n_a} P_{ij} Q_j - \sum_{j=1}^{n_i} P_{ij} Q_j &= 0 \\ (\varepsilon_i - \varepsilon_a) \sum_{j=1}^{n_e} f_{ij} Q_j + \varepsilon_i \sum_{j=1}^{n_a} f_{ij} Q_j - \varepsilon_a \sum_{j=1}^{n_i} f_{ij} Q_j &= \sigma(i) \end{aligned} \quad (23)$$

Where  $\varphi$  stands for electrode voltage,  $\varepsilon_i$  and  $\varepsilon_a$  represent the permittivity of insulator and air.  $P_{ij}$  and  $f_{ij}$  are the potential and normal flux density coefficients between  $i^{\text{th}}$  contour point and  $j^{\text{th}}$  simulated charge.  $\sigma$  is the charge density at  $i^{\text{th}}$  contour point of the rod model.

Dry conditions are simulated with an ideal external environment, which has no contamination and water. Therefore, surface resistivity is infinite.

$$I_r(t) = 0 \quad (24)$$

With DC voltage supply,

$$\sigma(i) = 0 \quad (25)$$

With AC voltage supply [13, 14, 32],

$$\sigma(i) = \frac{1}{S} \int I_c(t) dt \quad (26)$$

$$\begin{aligned} I_c(t) &= \frac{[\varphi(i-1) - \varphi(i)] - [\varphi(i) - \varphi(i+1)]}{j\omega C} \\ &= \frac{\varphi(i-1) + \varphi(i+1) - 2\varphi(i)}{j\omega C} \end{aligned} \quad (27)$$

$\varphi(i)$  represents the voltage at  $i^{\text{th}}$  contour point .  $C$  is the capacitance value between two contour points. AC angular frequency is  $\omega$  and surface area between contour points is  $S$ .

#### 4.3.2 GOVERNING EQUATIONS UNDER WET SURFACE CONDITIONS

On the electrode and air interface, the effects of charges in the electrode, charges in the insulator and all the charges in the water droplets must satisfy [9],

$$\sum_{j=1}^{n_e+n_i+n_w} P_{ij}Q_j = \varphi \quad (28)$$

On the electrode and insulator interface, the effects of charges in the electrode, charges in the air, and all the charges in the water droplets must satisfy,

$$\sum_{j=1}^{n_e+n_a+n_w} P_{ij}Q_j = \varphi \quad (29)$$

To establish potential and normal flux density continuity on the insulator-air interface, the effects of charges in the electrode, charges in the insulator, charges in the air, and charges in the water droplets must satisfy,

$$\sum_{j=1}^{n_a} P_{ij}Q_j - \sum_{j=1}^{n_i} P_{ij}Q_j = 0 \quad (30)$$

$$(\varepsilon_i - \varepsilon_a) \sum_{j=1}^{n_e+n_w} f_{ij}Q_j + \varepsilon_i \sum_{j=1}^{n_a} f_{ij}Q_j - \varepsilon_a \sum_{j=1}^{n_i} f_{ij}Q_j = \sigma(i) \quad (31)$$

Similarly, potential and normal flux density continuity on the insulator-water interface should be satisfied by following equations [20-21]:

$$\sum_{j=1}^{n_{sw}+n_a} P_{ij} Q_j - \sum_{j=1}^{n_i} P_{ij} Q_j = 0 \quad (32)$$

$$(\varepsilon_i - \varepsilon_w) \sum_{j=1}^{n_e+n_i+n_w-n_{sw}} f_{ij} Q_j + \varepsilon_i \sum_{j=1}^{n_{sw}} f_{ij} Q_j - \varepsilon_w \sum_{j=1}^{n_i} f_{ij} Q_j = \sigma(i) \quad (33)$$

Similarly, potential and normal flux density continuity on the air-water interface should be satisfied by following equations:

$$\sum_{j=1}^{n_{sw}} P_{ij} Q_j = 0 \quad (34)$$

$$(\varepsilon_i - \varepsilon_w) \sum_{j=1}^{n_e+n_i+n_w-n_{sw}} f_{ij} Q_j + \varepsilon_i \sum_{j=1}^{n_{sw}} f_{ij} Q_j - \varepsilon_w \sum_{j=1}^{n_a} f_{ij} Q_j = \sigma(i) \quad (35)$$

The charge density  $\sigma$  at  $i^{\text{th}}$  contour point of rod model can be expressed as [10]:

$$\sigma(i) = \frac{1}{S} \int_0^t I_i(t) \quad (36)$$

In wet conditions, surface resistivity is considered as surface resistivity  $\rho=10^6$   $\Omega \cdot m$  for the worst case assumption.

With DC voltage supply [15],

$$\begin{aligned} I_t(t) &= I_r(t) \\ &= \frac{\varphi(i-1) + \varphi(i+1) - 2\varphi(i)}{R} \end{aligned} \quad (37)$$

With AC voltage supply,

$$\begin{aligned} I_t(t) &= I_c(t) + I_r(t) \\ &= [\varphi(i-1) + \varphi(i+1) - 2\varphi(i)] \left( \frac{1}{j\omega C} + \frac{1}{R} \right) \end{aligned} \quad (38)$$

R is surface resistance,

$$R = \int_{i-1}^i \frac{\rho}{2\pi r} dl \quad (39)$$

In the equation (23),  $r$  is the radius of rod insulator model and  $\rho$  is surface resistivity.

Normal flux density between water-air interface changes with various geometries of water droplets, therefore, this flux density must be calculated accurately in 3D model.

Normal flux density of water droplets is shown in Figure 14.

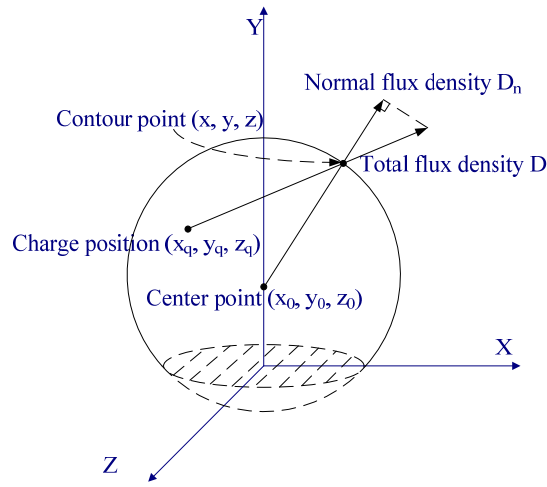


Figure 14. Normal flux density vector of water droplets

Since surface of water droplet description is given in equation (1), normal flux density direction is:

$$\vec{a} = (x - x_0)\vec{l} + (y - y_0)\vec{m} + (z - z_0)\vec{n} \quad (40)$$

Direction of total flux density generated by charges is:

$$\vec{F} = (x - x_q)\vec{l} + (y - y_q)\vec{m} + (z - z_q)\vec{n} \quad (41)$$

And then, normal flux density of water droplets is calculated with the following method.

Value of total flux density is:

$$D = \frac{Q}{4\pi[(x-x_q)^2 + (y-y_q)^2 + (z-z_q)^2]} \quad (42)$$

Therefore, normal flux density equals to:

$$D_n = D \frac{\vec{F} \cdot \vec{a}}{|\vec{F}| |\vec{a}|} = D \frac{\vec{F} \bullet \vec{a}}{|\vec{F}| |\vec{a}|} \quad (43)$$

## 5. ELECTRIC POTENTIAL AND FIELD ANALYSIS

### 5.1 Introduction

Electric potential and field distributions along the insulator surfaces are the basic standards to evaluate the corona and flashover phenomena. Therefore, the fields are calculated under dry and wet conditions. Under dry conditions, the insulators for AC and DC lines with various voltage levels are analyzed. Under wet conditions, the separation of water droplets on the insulator surface is the main factor to affect the field strength. Therefore, different separations of water droplets are simulated. The maximum electric field strength, as a function of spaces between water droplets, is also calculated.

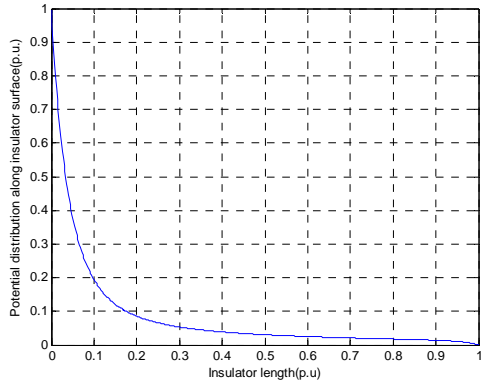
### 5.2 Simulating results under dry conditions

#### 5.2.1 HVAC insulators

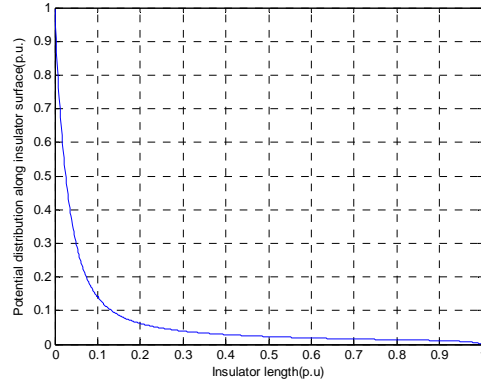
The insulator dimensions of 500 kV – 1200 kV HVAC insulators are shown in table I [1]. The corona threshold in dry conditions is 15.2 kV/cm [17].

Table 1 The dimension for AC composite insulators

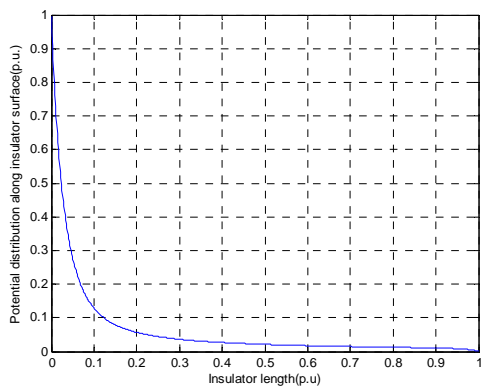
Voltage rating (kV)	Dry arc distance (mm)	Leakage distance (mm)
500	5000	13750
765	6600	23500
1000	7110	25550
1200	8530	30660



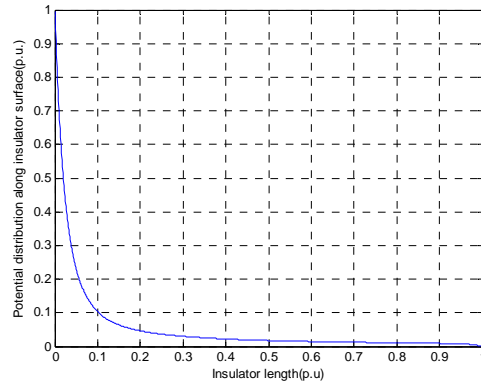
(a)



(b)



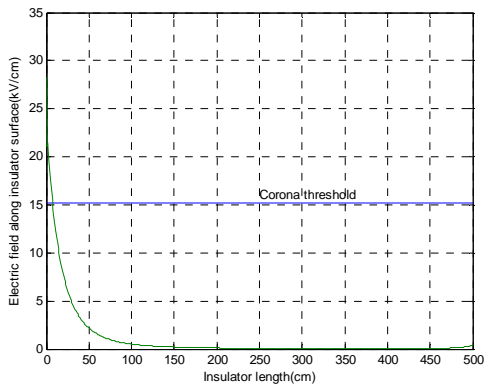
(c)



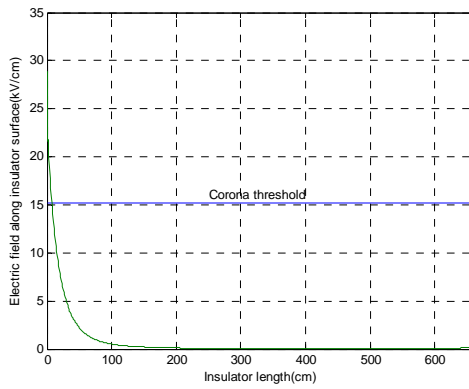
(d)

Figure 15. Potential distribution along HVAC insulator surfaces under dry conditions. The voltage levels are (a) 500 kV, (b) 765 kV, (c) 1000 kV and (d) 1200 kV respectively.

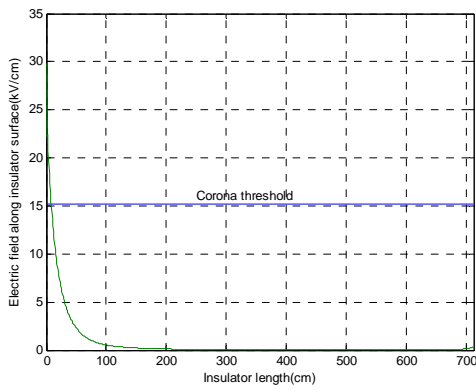
Figure 15 shows the potential distribution along the insulator surface with AC supply voltage. Four voltage levels are simulated, and the insulator lengths are normalized. It can be observed that potential distribution becomes more and more nonlinear as the voltage level climbs.



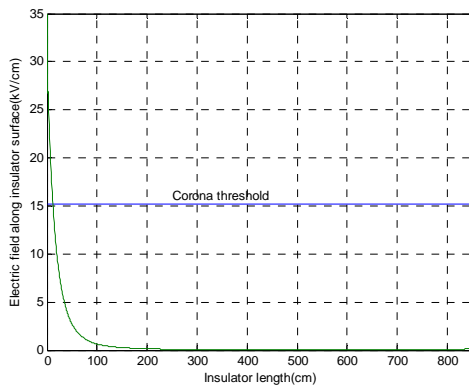
(a)



(b)



(c)



(d)

Figure 16. Electric field distribution along HVAC insulator surfaces under dry conditions. The voltage levels are (a) 500 kV, (b) 765 kV, (c) 1000 kV and (d) 1200 kV respectively.

Figure 16 shows the electric field distribution along insulator surface with AC supply voltage. Comparing field distribution plots of all voltage levels with corona threshold inception, it can be shown that the length of the insulator surface where could produce corona increases with voltage levels.

### 5.2.2 HVDC insulators

With DC voltage supply, the density of free electrons with negative DC voltage is higher than it with positive DC voltage supply. The free electrons have collisions with air molecules, enhancing the ionization in the corona area, which leads to the increase of ionized currents. Therefore, in the equation of normal flux continuity boundary condition, the charge density between the insulator and air interface is negative and higher [3, 31].

The electric potential and field distribution is shown Figure 17 and Figure 18.

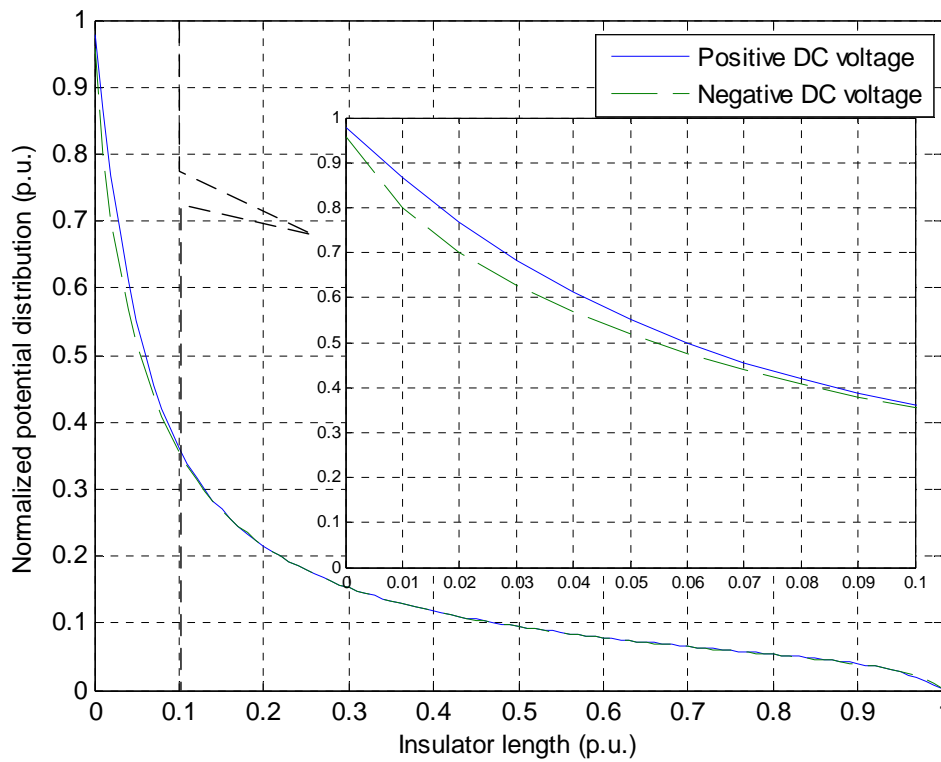


Figure 17. Normalized positive and negative DC potential distribution

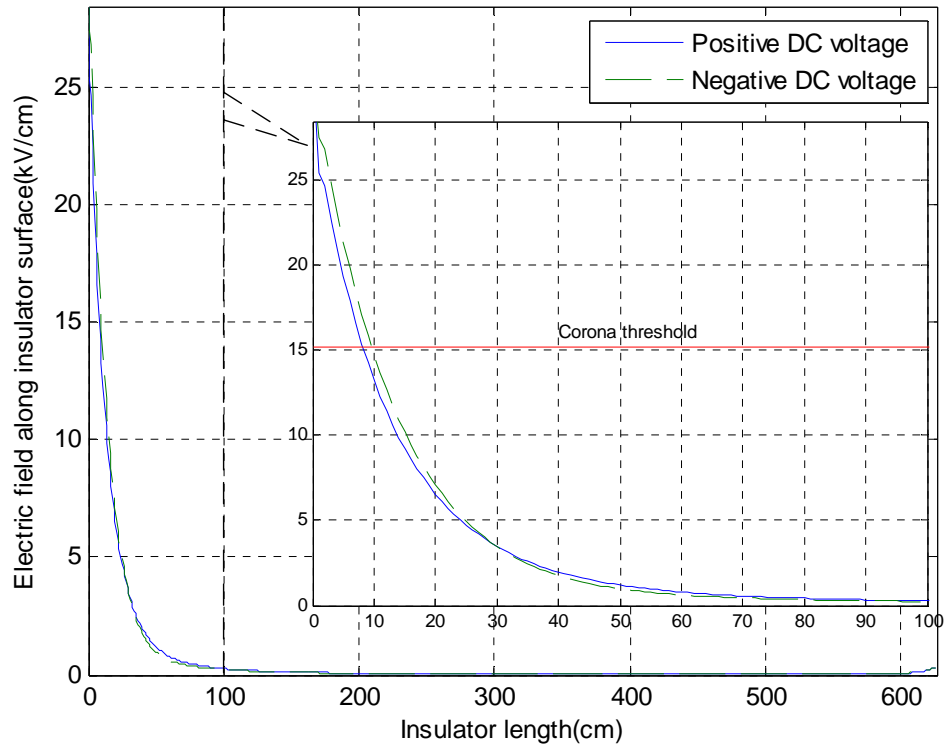


Figure 18. Normalized positive and negative DC electric field distribution

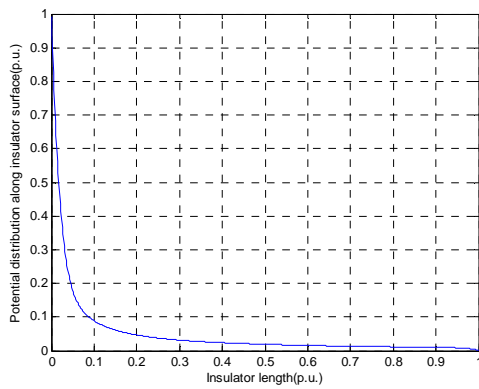
Figure 18 shows electric field distribution of positive and negative DC supply voltage at 500 kV level. In order to make the plot clear, 10% length of the insulator close to HV electrode is enhanced. It is concluded that the maximum field strength of negative polarity is higher than the positive polarity, and the negative field distribution is more nonlinear than the positive field distribution. Therefore, the calculation of electric potential and field distribution is based on the negative polarity, in order to achieve the margin field strength in the worst case assumption.

The insulator dimensions of 500 kV – 1200 kV HVDC insulators are shown in table

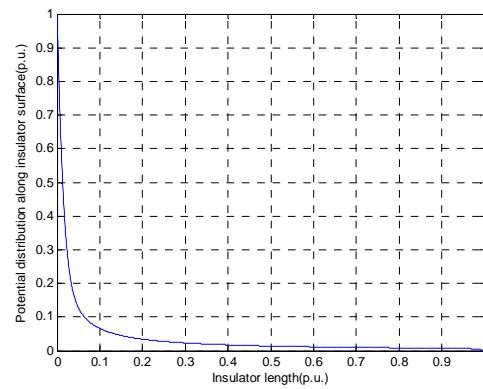
II [1].

Table 2 The dimension for DC composite insulators

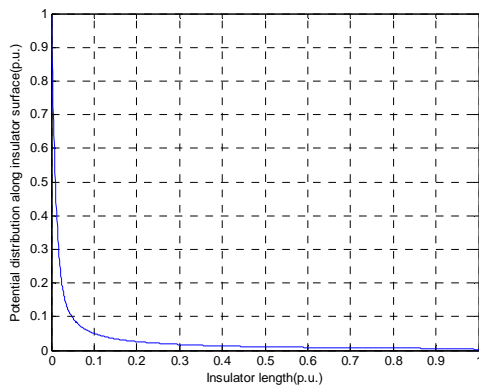
Voltage rating (kV)	Dry arc distance (mm)	Leakage distance (mm)
500	6250	15938
800	8600	29375
1000	11500	31938
1200	15000	38325



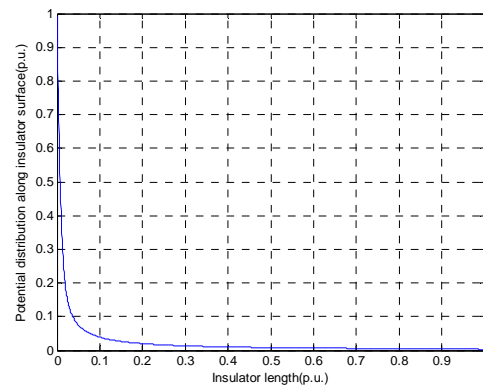
(a)



(b)

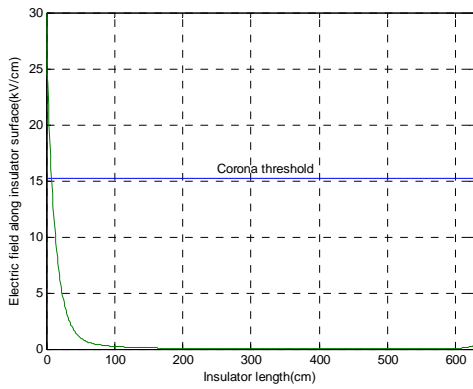


(c)

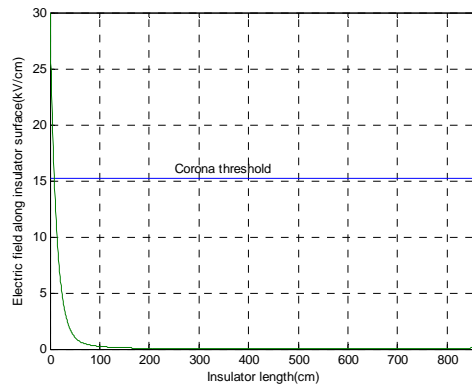


(d)

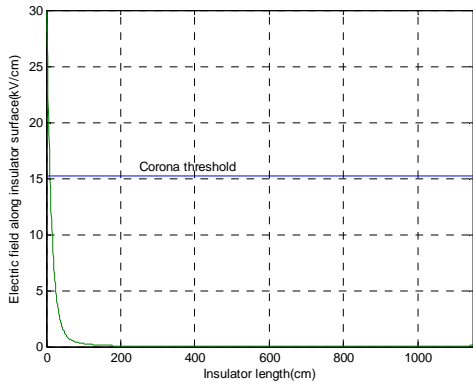
Figure 19. Potential distribution along HVDC insulator surfaces under dry conditions. The voltage levels are (a) 500 kV, (b) 765 kV, (c) 1000 kV and (d) 1200 kV respectively.



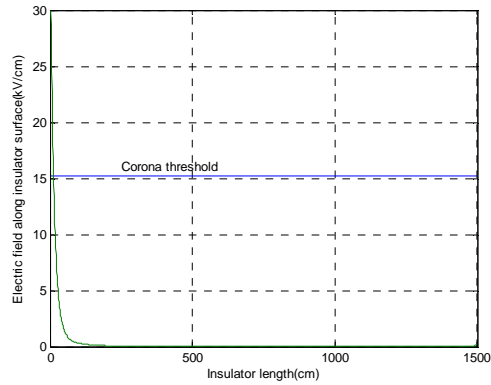
(a)



(b)



(c)



(d)

Figure 20. Electric field distribution along HVDC insulator surfaces under dry conditions. The voltage levels are (a) 500 kV, (b) 765 kV, (c) 1000 kV and (d) 1200 kV respectively.

Figure 19 and Figure 20 show the electric potential and field distribution at different voltage levels, respectively. The nonlinearity increases when the voltage level climbs. Meanwhile, the length of the insulator surface that could create corona rises with voltage levels.

### 5.2.3 Comparison between HVDC and HVAC insulators

Figure 21 shows that potential distribution of AC and DC supply voltage at 500 kV level. It indicates that the DC potential distribution is more nonlinear than AC voltage distribution.

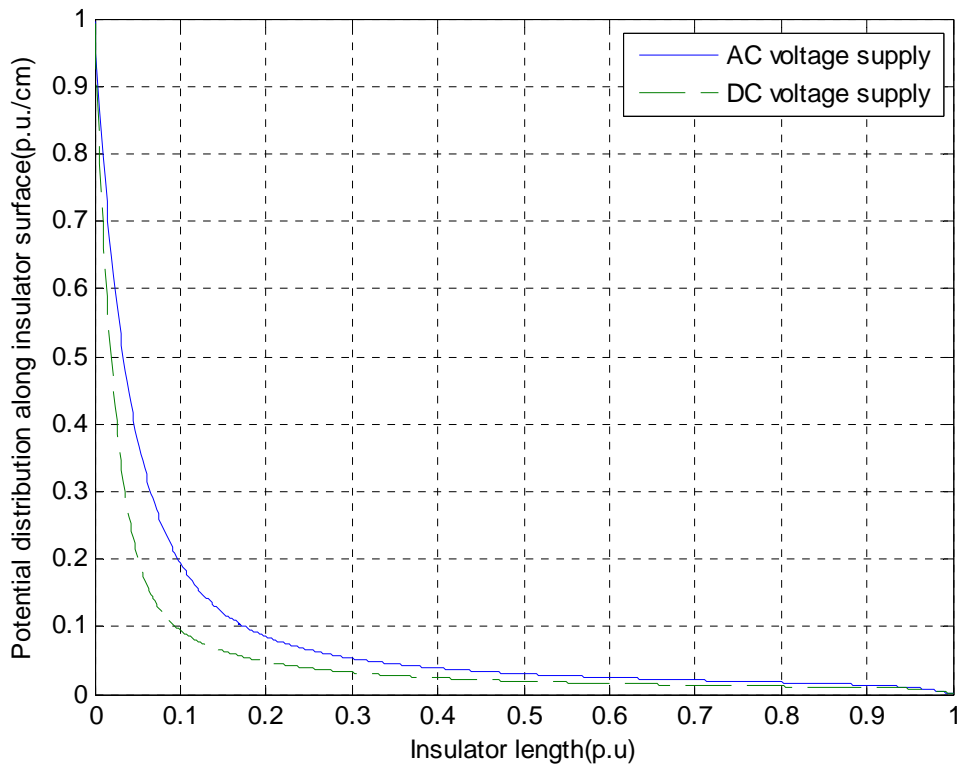


Figure 21. Normalized AC and DC potential distribution

Figure 22 shows that DC electric field strength is higher than AC in the part of insulator, whose field strength is above corona threshold. Therefore, the DC insulator is more likely to create corona than the AC. Figure 22 shows that the maximum AC and DC insulator field strength are 18.39 kV/cm and 27.75 kV/cm, respectively.

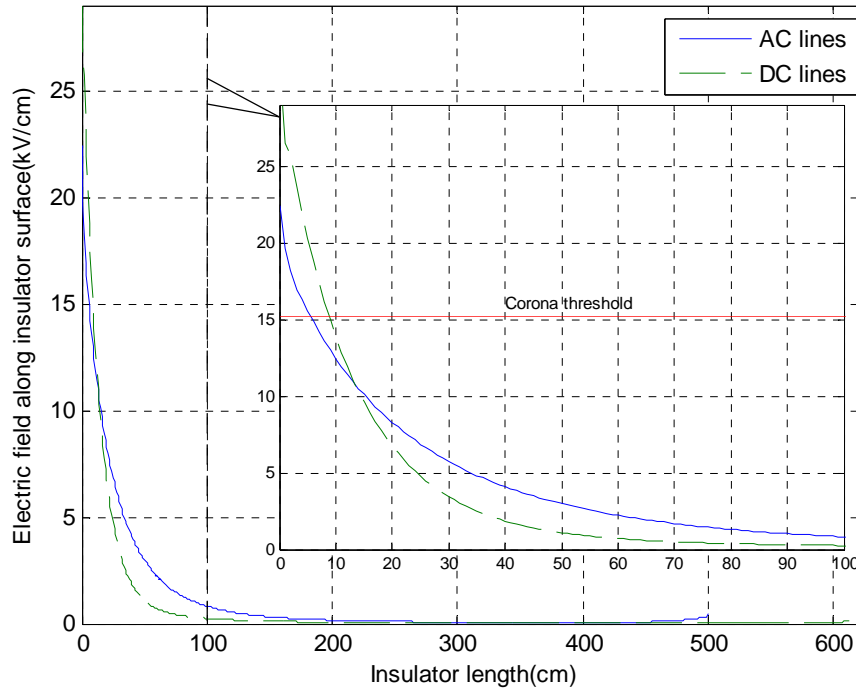


Figure 22. Normalized AC and DC electric field distribution

### 5.3 Simulating results under wet conditions

Water droplets distribution on the 500 kV voltage level insulator surface is simulated in this section. The maximum dry arc distance of insulators that can be handled by mobile work station is six meters, for limited computation resources and accuracy requirement.

The inception field strength of streamer propagation on the wet surface of insulators is 4 kV/cm [16, 17], and surface resistivity between materials interface is assumed at  $10^6$   $\Omega$ -m. From previous work [10], the maximum electric field strength is in reverse

proportion to spaces between droplets. Therefore, small spaces are used to estimate the maximum electric field strength.

### 5.3.1 HVAC insulators

Table 3 shows water droplets arrangements with AC voltage.

Table 3 Arrangement of water droplets with AC voltage supply

Voltage levels of the insulators (kV)	Radius of each water droplets (mm)	Space between water droplets (mm)	Number of water droplets
500	2.5	2.5	1000

Figure 23 shows the electric field distribution with 500 kV AC supply voltage. 11% length of insulator close to HV electrode is capable to generate corona. The maximum electric field strength aroused by water droplets is 27.73 kV/cm.

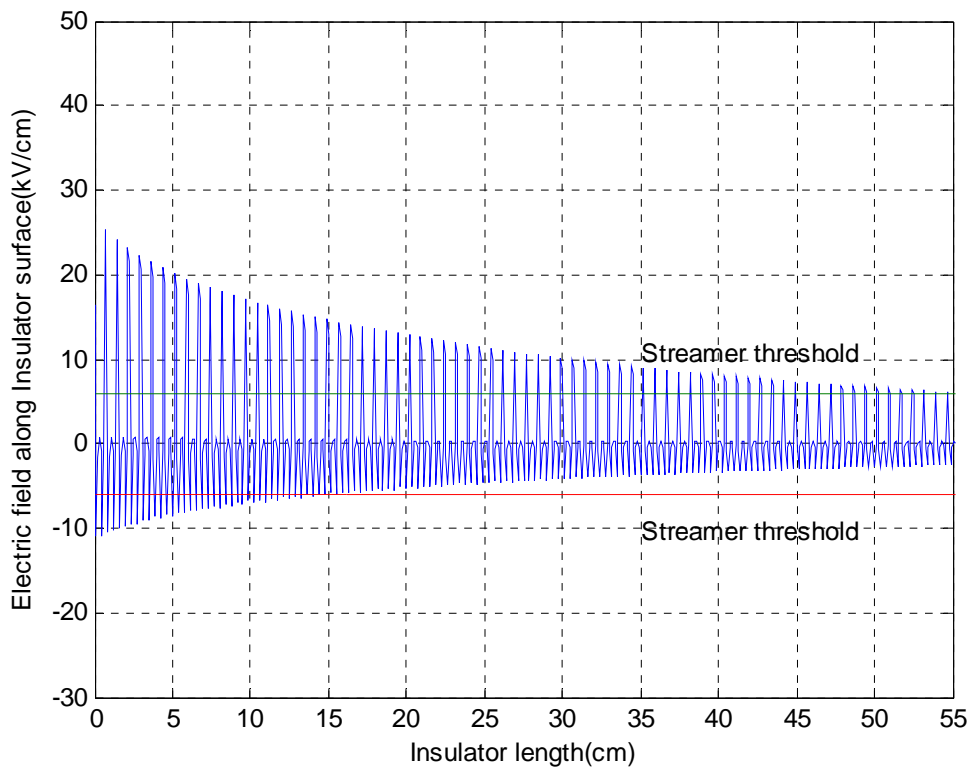


Figure 23. Electric field distribution along HVAC insulator surfaces under wet conditions.

### 5.3.2 HVDC insulators

Table 4 shows water droplets arrangements with DC voltage.

Table 4 Arrangement of water droplets with DC voltage supply

Voltage levels of the insulators (kV)	Radius of each water droplets (mm)	Space between water droplets (mm)	Number of water droplets
500	2.5	2.5	1350

Figure 24 and Figure 25 show the electric field distribution with DC supply voltage.

With positive polarity, 16.0 % length of insulator close to HV electrode is capable to generate corona, while 19.2% length of insulator close to HV electrode is capable to generate corona with negative polarity. The maximum electric field strengths aroused by water droplets, under positive and negative voltage supply, are 31.3 kV/cm and 33.6 kV/cm.

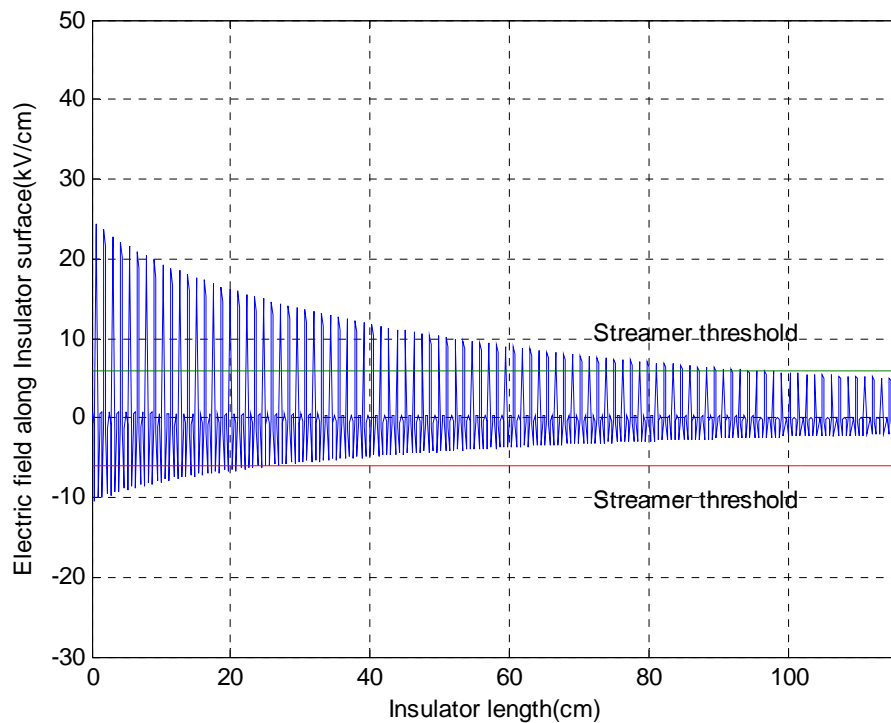


Figure 24. Electric field distribution with water droplets and +500 kV DC voltage

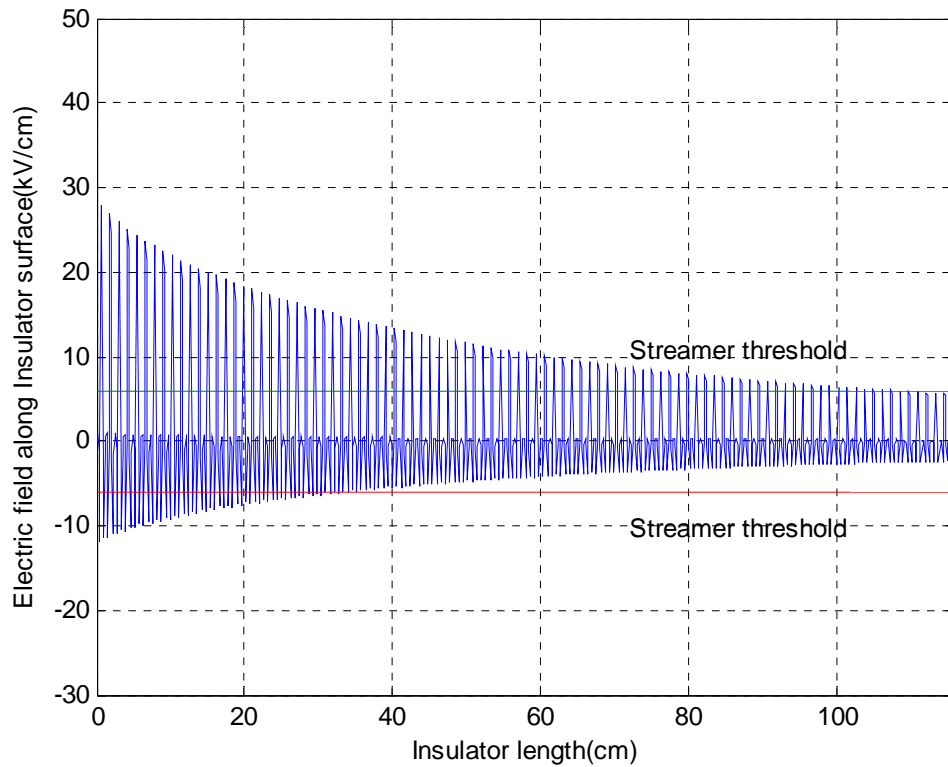


Figure 25. Electric field distribution with water droplets and -500 kV DC voltage

### 5.3.3 Effects of space between water droplets

In this section, effects of gap between water droplets are simulated on the 500 kV HVDC insulators.

Table 5 Four cases of different gaps between water droplets

	Radius of each water droplets (mm)	Space between water droplets (mm)	Number of water droplets
Case 1	2.5	2.5	1250
Case 2	2.5	12.5	416
Case 3	2.5	25	208
Case 4	2.5	50	104

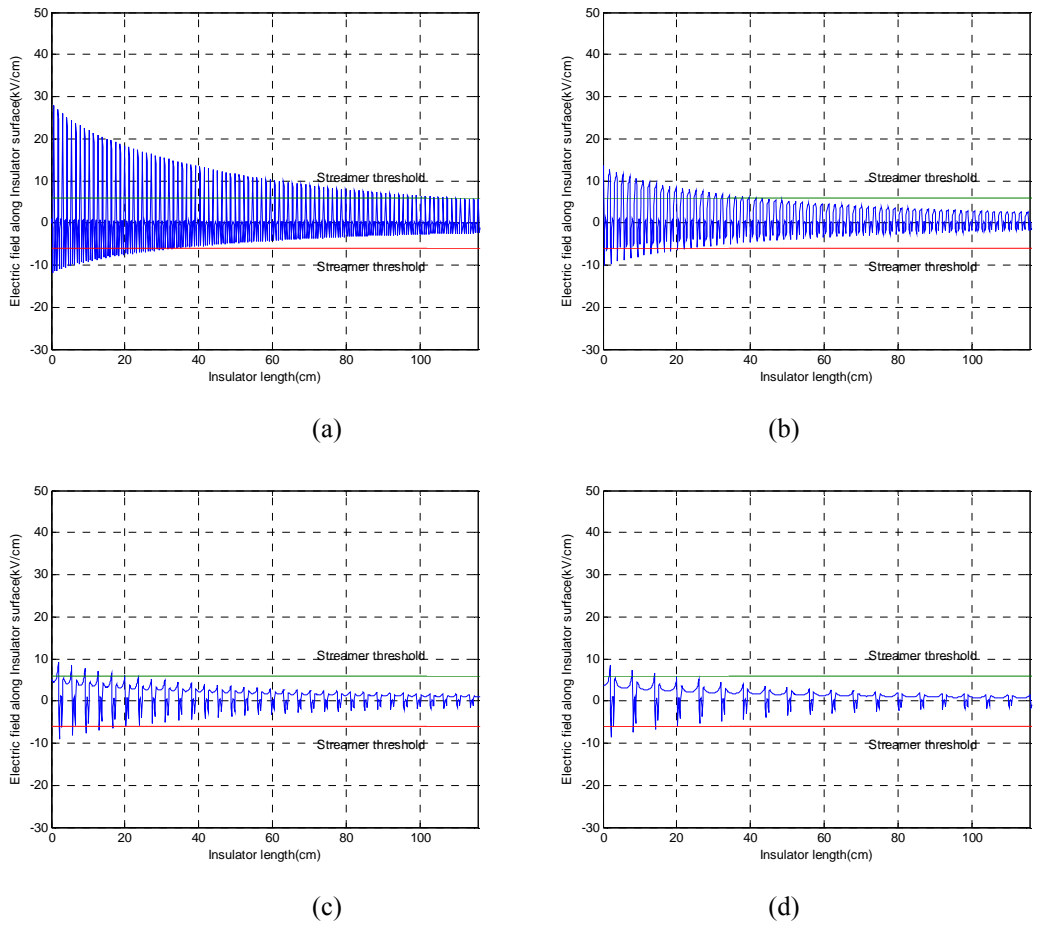


Figure 26. Electric field distribution with different spaces between water droplets.  
 (a) space is 2.5 mm, (b) space is 7.5 mm, (c) space is 12.5 mm and (d) space is 17.5 mm

Figure 26(a) shows that 19.2% insulator close to HV (high voltage) electrode is capable to generate corona. Figure 26(b) shows that 6.4% insulator close to HV (high voltage) electrode is capable to generate corona. Figure 26(c) shows that 2.9% insulator close to HV (high voltage) electrode is capable to generate corona, and Figure 26(d) shows that 1.3% insulator close to HV (high voltage) electrode is capable to generate corona. The maximum electric field strength aroused by water droplets is 33.6 kV/cm, 32.4 kV/cm, 27.2 kV/cm and 25.3 kV/cm, respectively.

The maximum electric field distribution as a function of gaps between water droplets are shown in Figure 27. Therefore, it is concluded that electric field strength caused by each water droplet reduces as the space between water droplets increases.

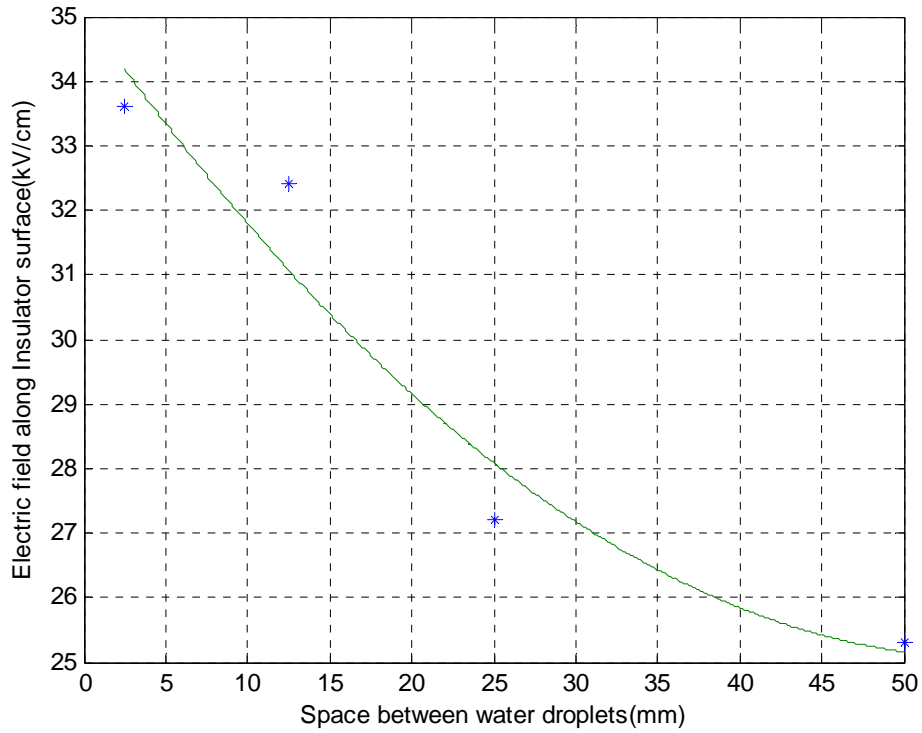


Figure 27. The maximum electric field distributions as a function of spaces between water droplets

## 6. OPTIMIZATION OF GRADING RINGS

### 6.1 Introduction

In this chapter, both corona rings and grading rings are utilized to reduce the occurrences of corona phenomena at the 500 kV transmission lines. The ring radius, ring tube thickness, and the projection of ring from end-fittings are the three main factors to affect the corona and grading rings performance [26, 28].

The optimization method of the three factors is given in [17]. The corona rings are set at the electrode with certain ring radius and tube thickness from the design manual [7]. The grading rings are then optimized to minimize the electric field along the insulator surface. The structure of corona and grading rings is shown in Figure 28.

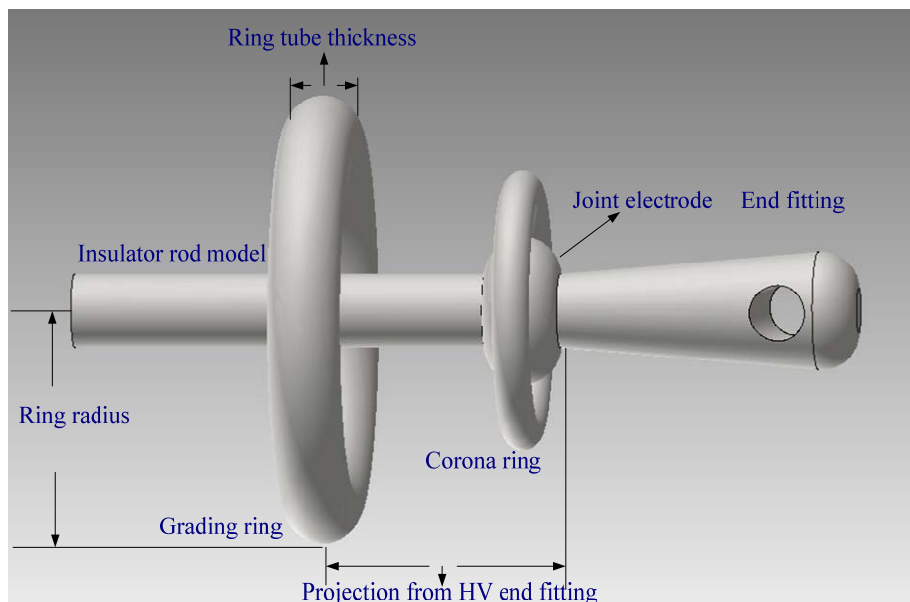


Figure 28. Cross section schematic of rod insulator model with corona and grading rings

## 6.2 Grading ring optimization under dry conditions

### 6.2.1 Optimization for HVAC insulators

The evaluation of one factor is made while two other factors are fixed. By using this method, the optimized corona ring radius, tube thickness and projection are 30 cm, 5 cm, and 0 cm, respectively [16]. The grading rings are then optimized, and the least square method is employed to obtain the second order function by the discrete points. The effect of ring radius on electric field distribution is shown in Figure 29.

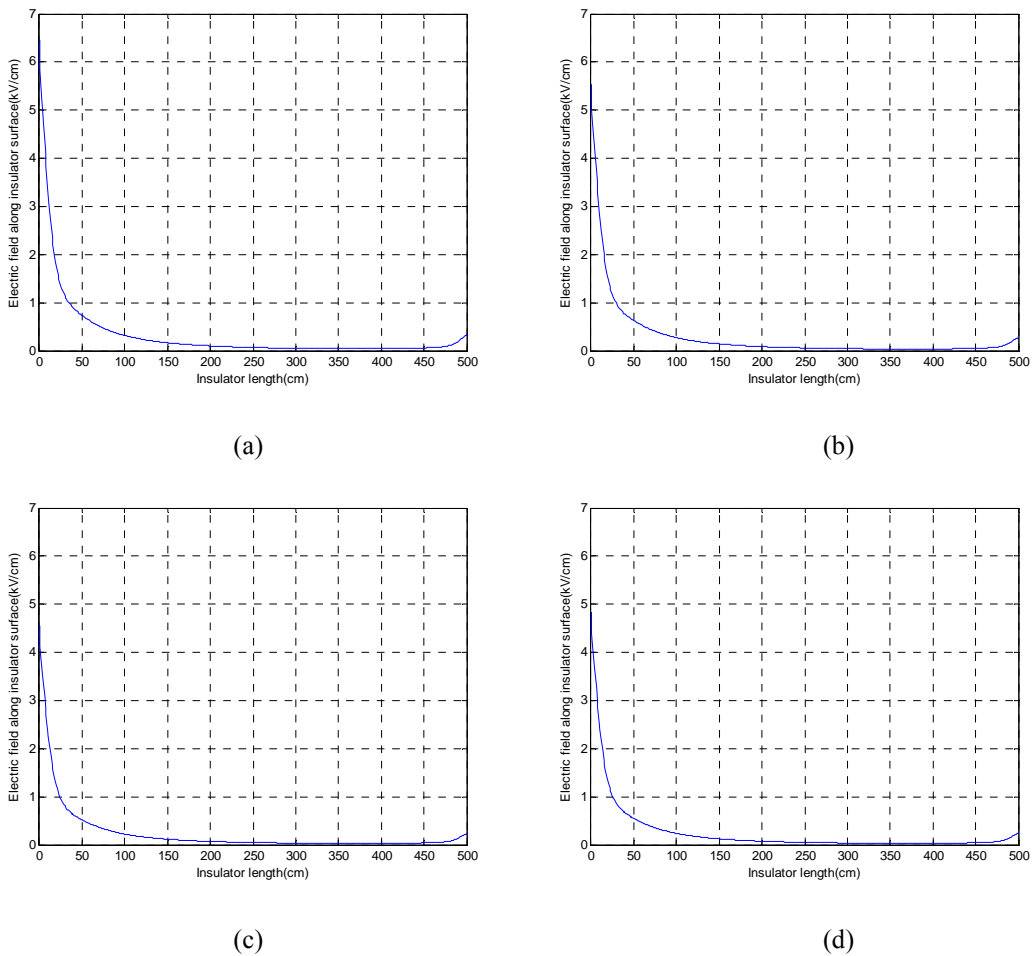


Figure 29. Impact of grading ring radius on field distribution with AC voltage supply  
Radius is 30 cm, (b) Radius is 40 cm, (c) Radius is 50 cm, (d) Radius is 60 cm

The maximum electric field distribution as a function of ring radius is shown in Figure 30. It can be concluded that the optimized ring radius is 53 cm.

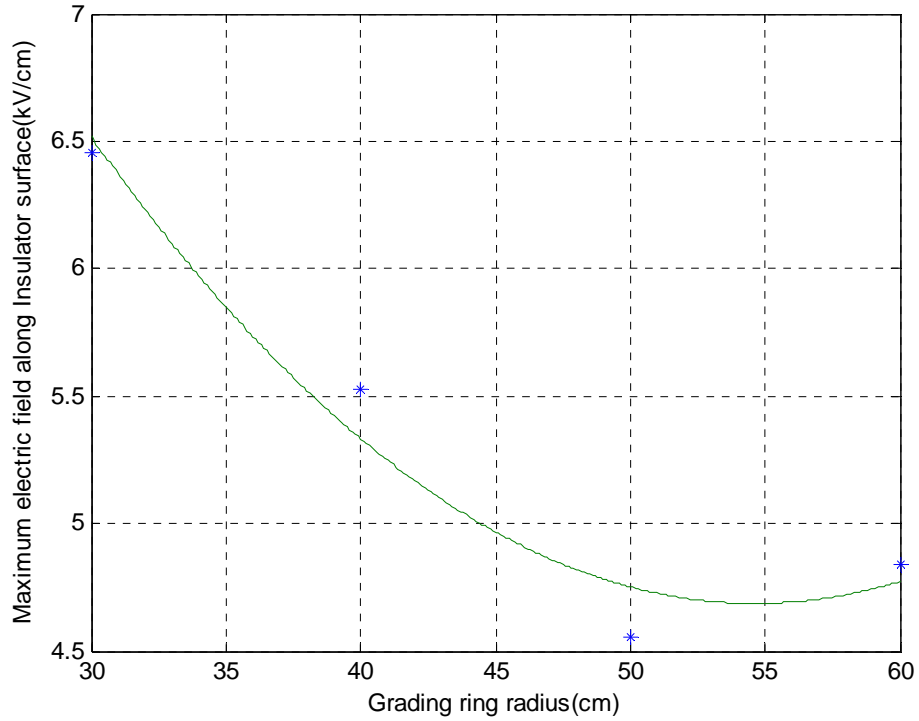
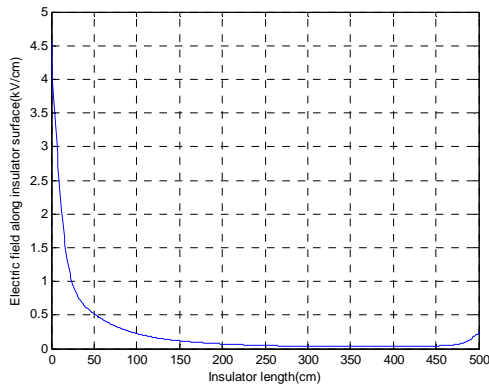
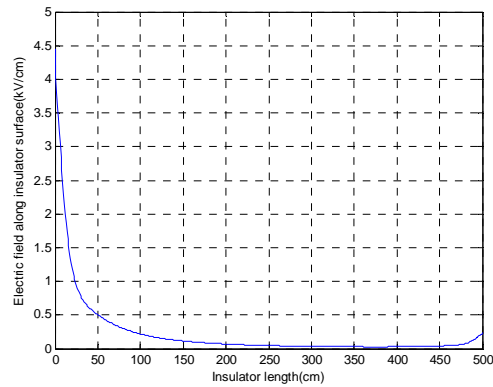


Figure 30. Maximum electric field as a function of ring radius of the HVAC insulator

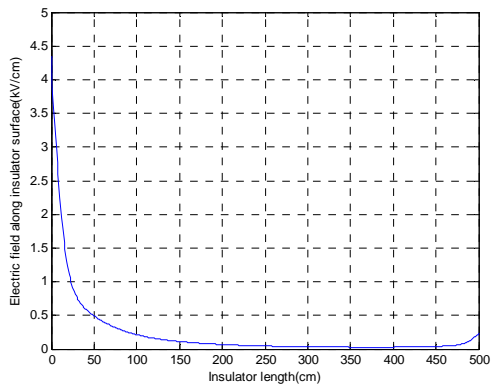
The second step is to evaluate the effect of the ring tube thickness on electric field distribution, while the radius is 53 cm and projection is 0 cm.



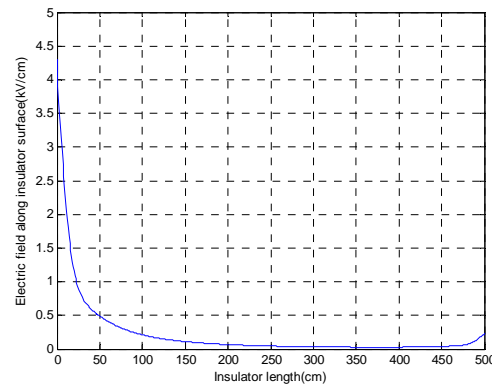
(a)



(b)



(c)



(d)

Figure 31. Impact of grading ring tube thickness on field distribution with AC voltage supply. (a) Tube thickness is 4 cm, (b) Tube thickness is 6 cm, (c) Tube thickness is 8 cm and (d) Tube thickness is 10 cm

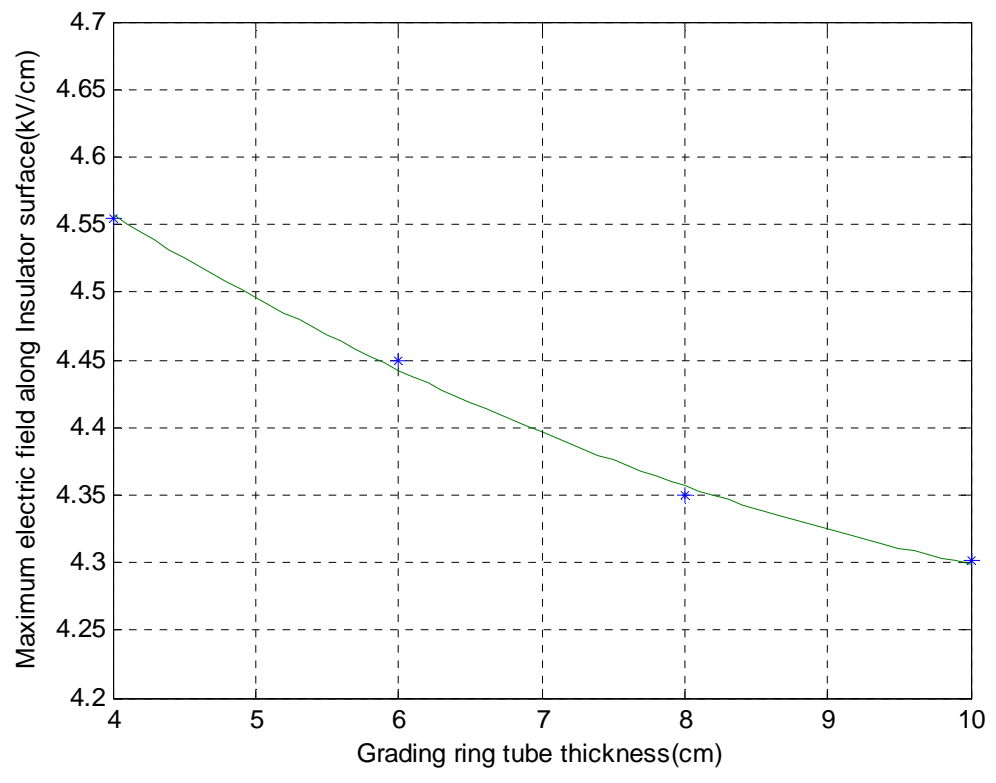


Figure 32. Maximum electric field as a function of tube thickness of the HVAC insulator

The maximum electric field distribution, as a function of tube thicknesses of corona rings, is shown in Figure 32. It can be concluded that the optimized tube thickness of corona rings is 10 cm.

The third step is to evaluate the effect of projections from the end-fittings on electric field distribution.

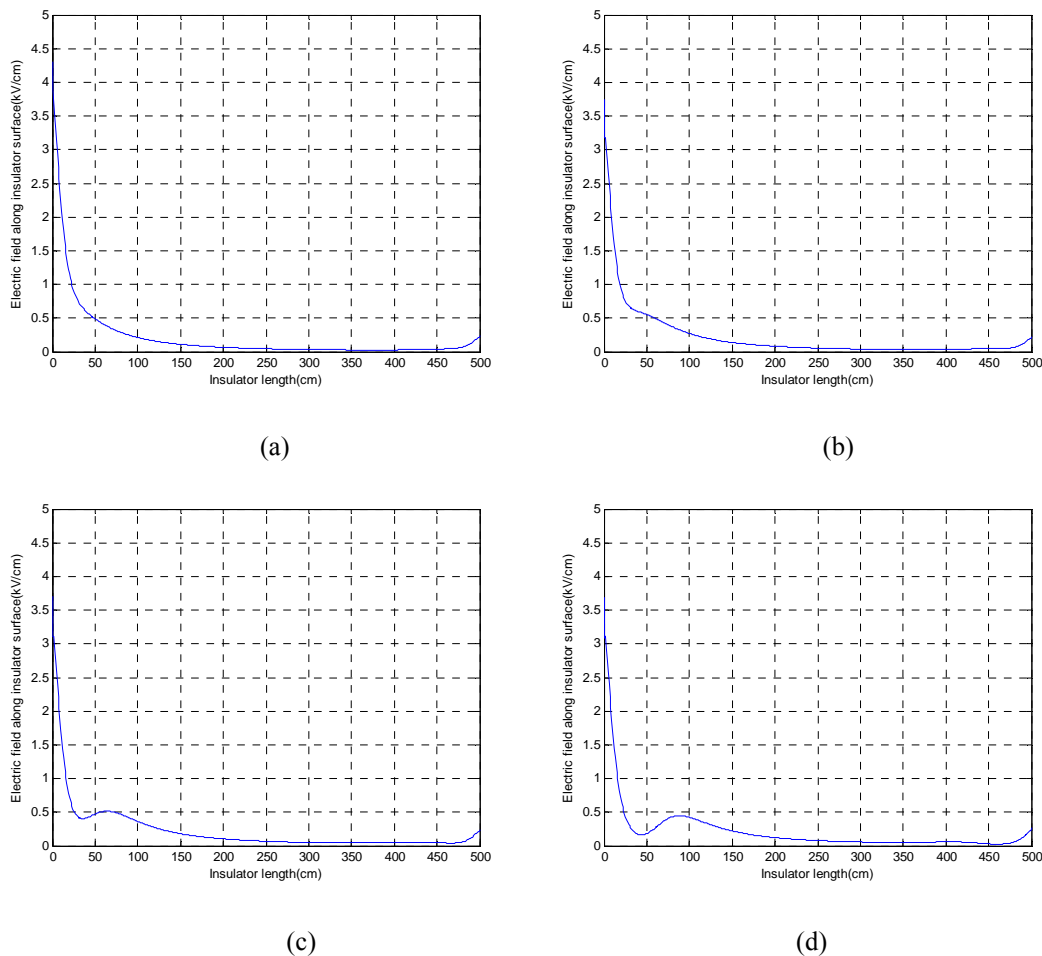


Figure 33. Impact of projection from the end-fitting on field distribution with AC voltage supply  
 (a) Projection is 0 cm, (b) Projection is 20 cm, (c) Projection is 40 cm and (d) Projection is 60 cm

Similarly, the projections from the end-fittings are measured. The maximum electric field distribution, as a function of projections from the end-fitting, is shown in Figure 33.

It can be concluded that the optimized projection of grading rings is 42 cm. From Figure 30, and Figure 32, and Figure 34, it indicates that ring radius is the major factor to affect grading ring performance, while ring tube thickness and projection slightly affect the field distribution. The electric field distribution with the optimized corona and grading rings is shown in Figure 34.

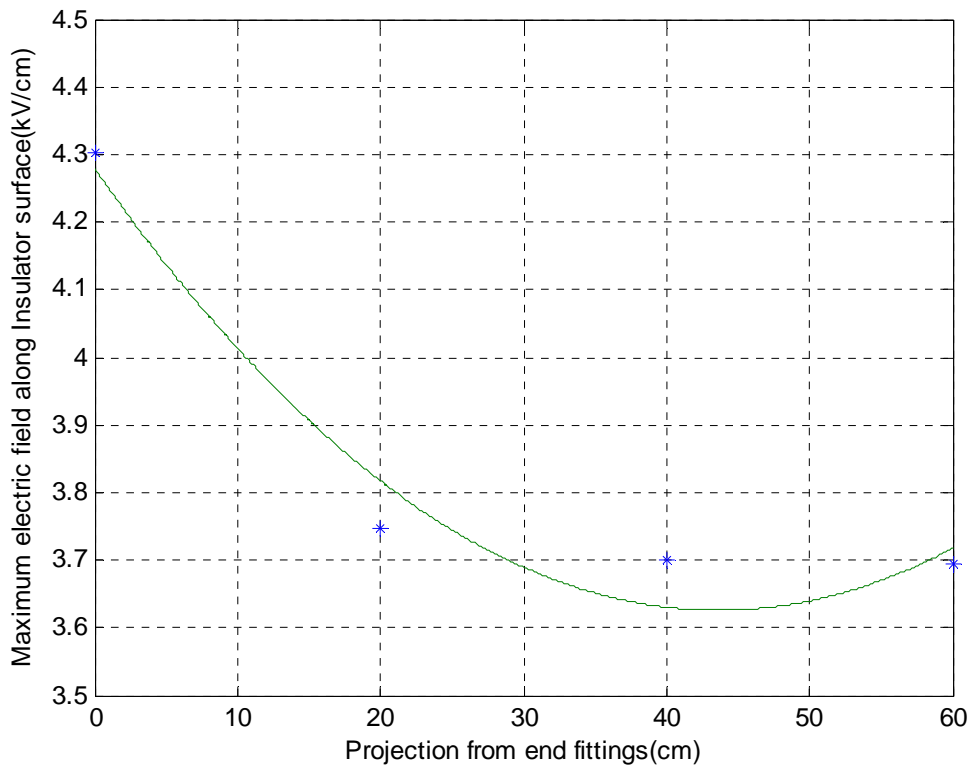


Figure 34. Maximum electric field as a function of projection of the HVAC insulator

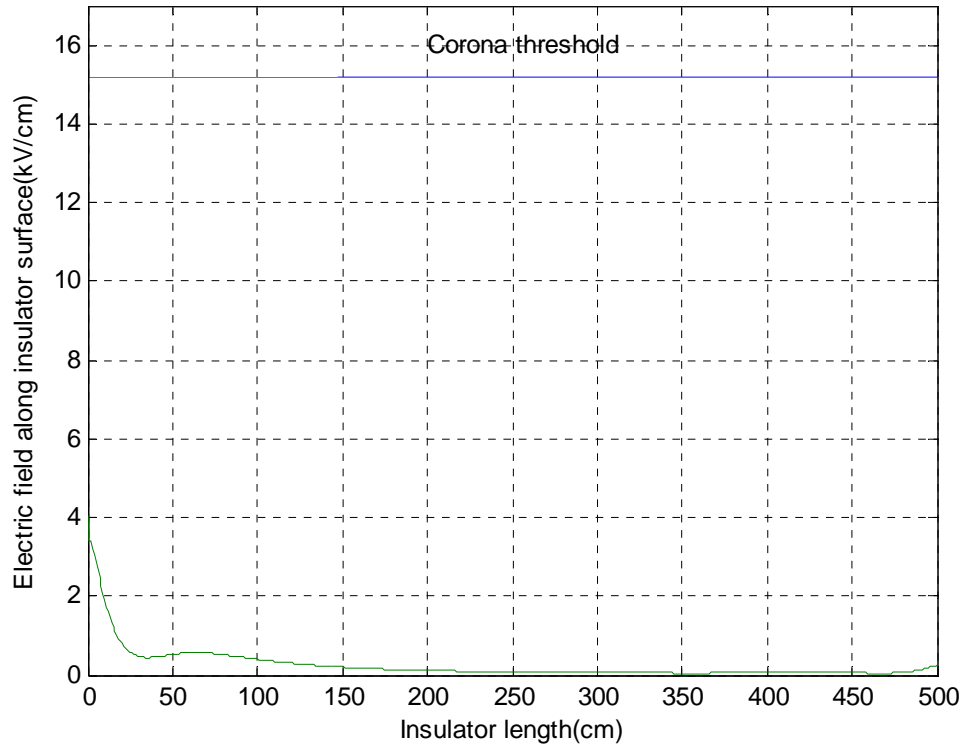


Figure 35. Electric field distribution along HVAC insulator surfaces with optimized corona and grading rings

### 6.2.2 Optimization for HVDC insulators

Since the electric field strength of negative polarity is higher than positive polarity, the corona and grading rings designs are based on the negative field distribution. Firstly, the grading and corona rings with optimized parameters under HVAC condition are put on the negative 500 kV HVDC line, to test whether the HVAC grading ring parameters can or cannot fit the HVDC insulator. The electric field distribution along the insulator surface is shown in Figure 34.

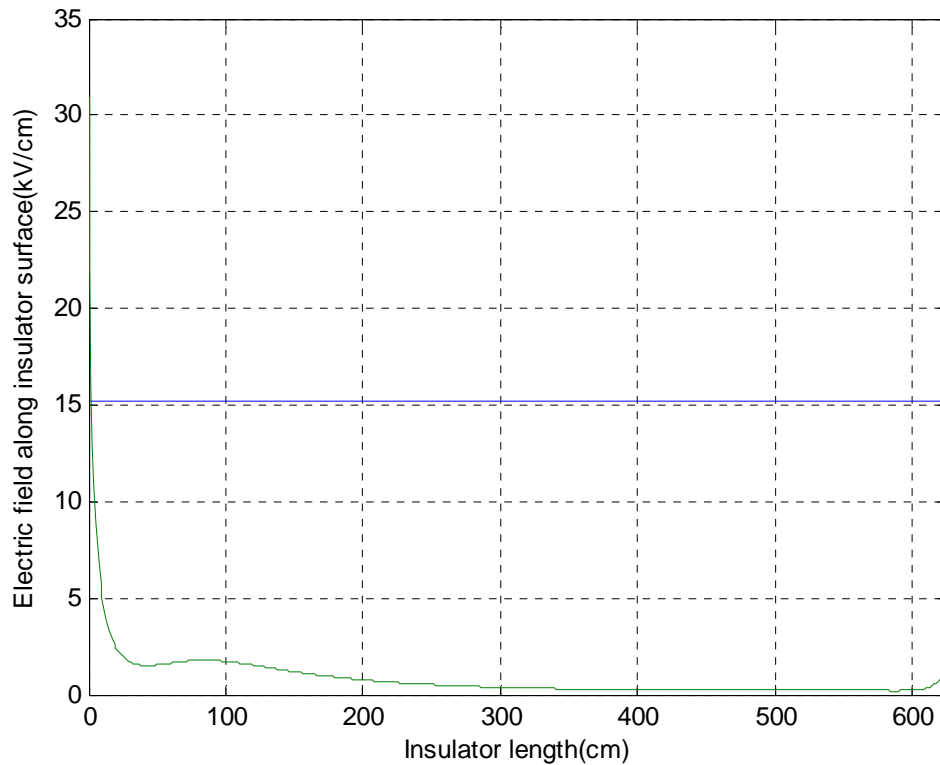


Figure 36. Electric field distribution along the insulator surface with HVAC corona and grading rings under -500 kV voltage supply

Figure 36 shows that the maximum electric field close to high voltage electrode exceeds the corona threshold. Therefore, the optimization process needs to be repeated. Since the grading rings parameters are the dominant factors that affect the field distribution, the parameters of corona rings remain the same.

The similar method is used in the process of grading rings optimization. One factor varies when other two factors are set as constant. Figure 37 shows the electric field distribution with different ring radiuses, while the tube thickness is 8 cm and the projection is 0 cm. Figure 39 shows the electric field distribution with different tube thicknesses, while the ring radius is 64 cm and the projection is 0 cm. Figure 41 shows

the electric field distribution with different projections from end fitting, while the ring radius is 64 cm and the tube thickness is 8 cm.

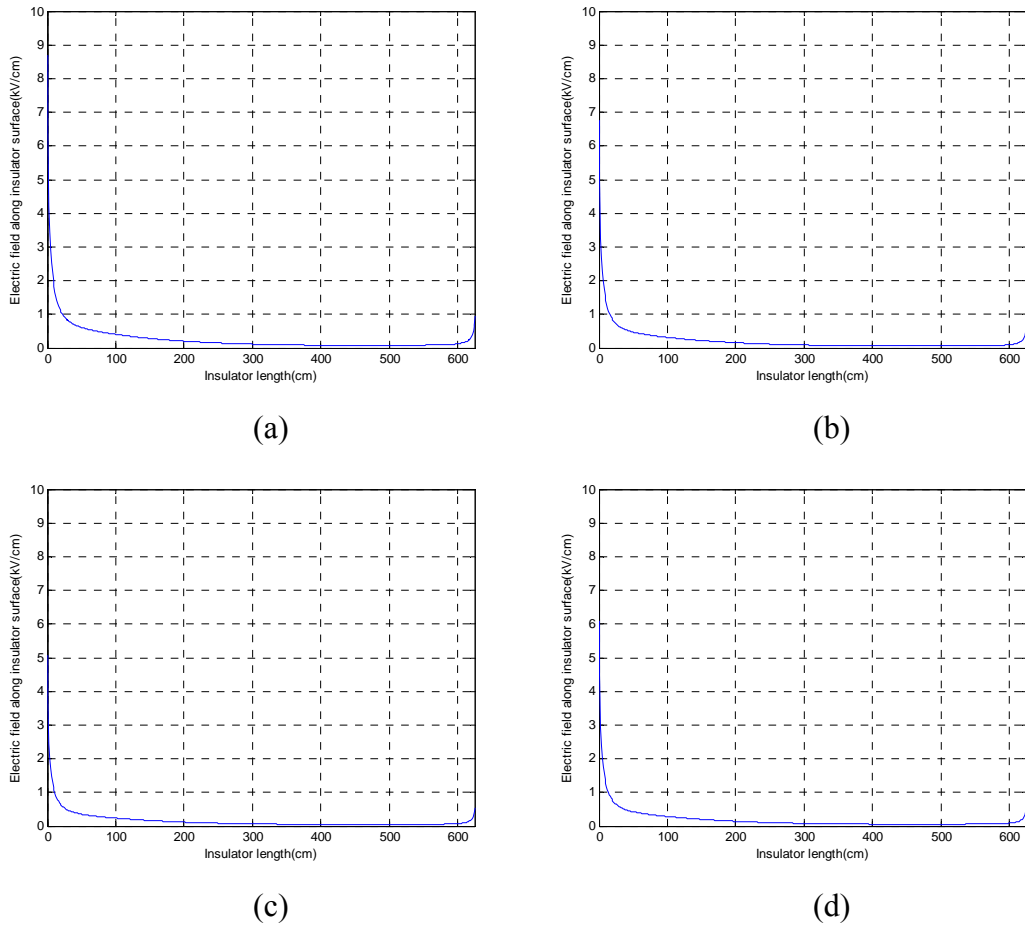


Figure 37. Impact of grading ring radius on field distribution with DC voltage supply  
 (a) Radius is 40 cm, (b) Radius is 50 cm, (c) Radius is 60 cm and (d) Radius is 70 cm

The maximum electric field distributions as a function of ring radius of grading rings are shown in Figure 38.

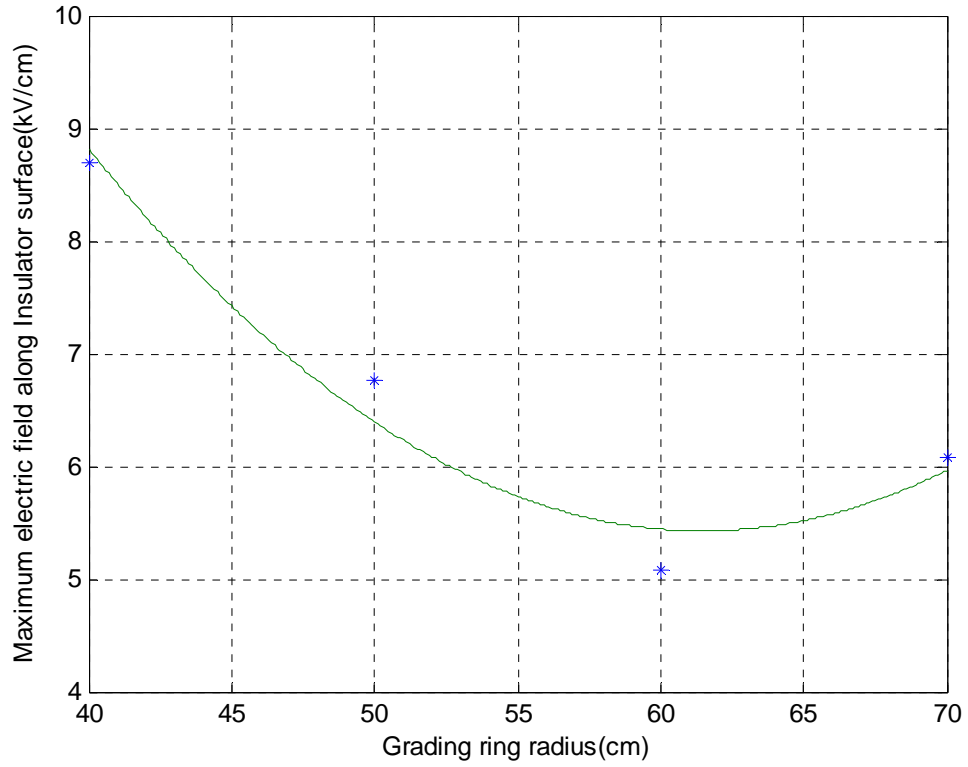
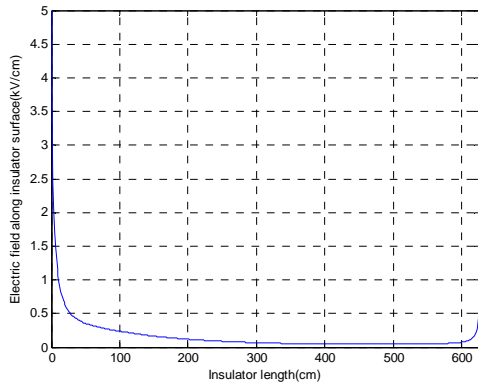
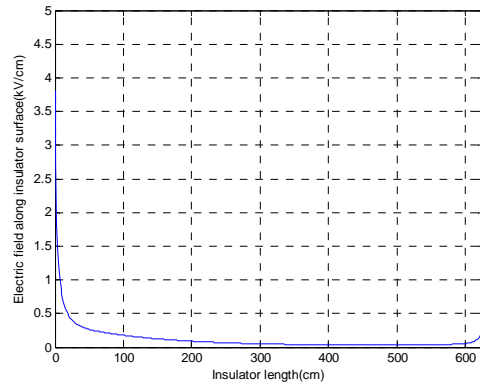


Figure 38. Maximum electric field as a function of radius of the HVDC insulator

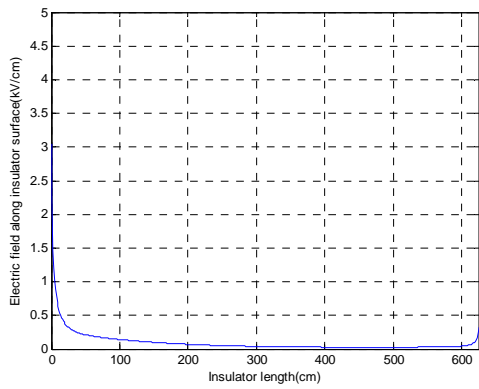
Figure 37 and Figure 38 indicate that the optimized ring radius is 64 cm with the DC voltage. The electric field distributions with different tube thickness are shown in Figure 39. The maximum electric field distributions as a function of tube thicknesses of grading rings are shown in Figure 40.



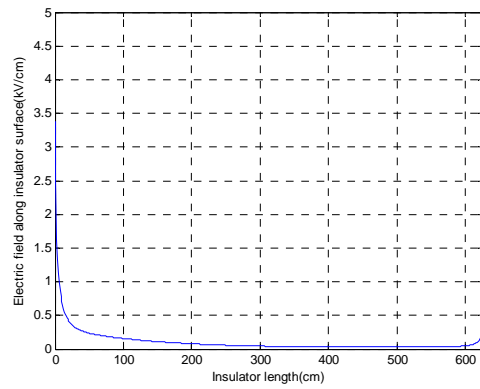
(a)



(b)



(c)



(d)

Figure 39. Impact of tube thickness on field distribution with DC voltage supply. (a) Tube thickness is 8 cm, (b) Tube thickness is 10 cm, (c) Tube thickness is 12 cm and (d) Tube thickness is 14 cm.

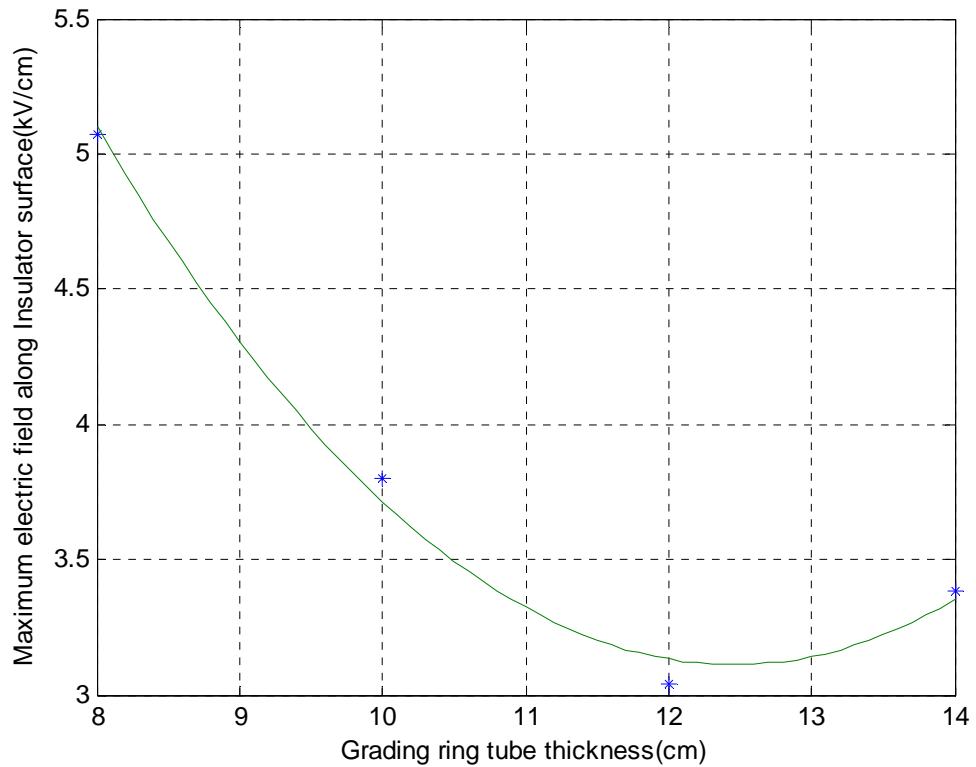
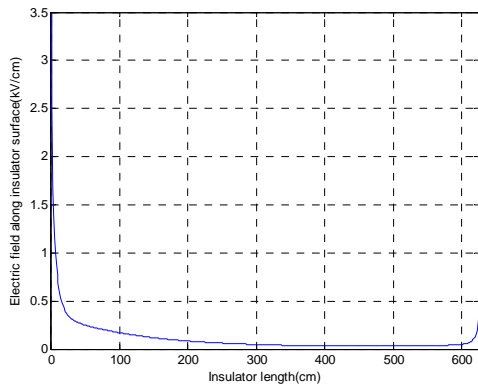
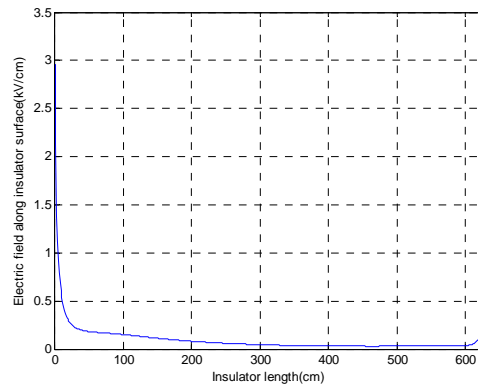


Figure 40. Maximum electric field as a function of tube thickness of the HVDC insulator

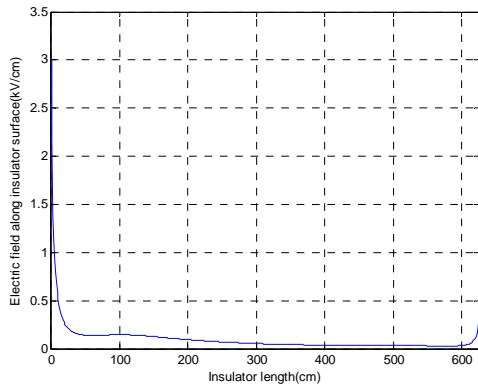
Figure 39 and Figure 40 indicate that the optimized tube thickness is 12.5 cm with the DC voltage. The electric field distributions with different projections from the end-fittings are shown in Figure 41.



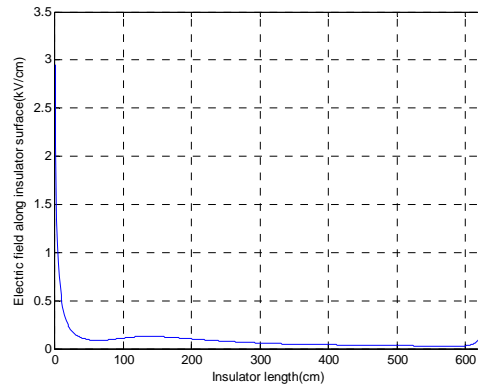
(a)



(b)



(c)



(d)

Figure 41. Impact of projection from end fitting on field distribution with DC voltage supply  
 (a) Projection is 0 cm, (b) Projection is 20 cm, (c) Projection is 40 cm and (d) Projection is 60 cm.

Compared to the HVAC insulator, the radius of grading ring is larger and tube thickness increases as well. Figure 42 indicates that the projection from end fitting does not affect the maximum electric field. However, Figure 41 shows that the relatively large projection can mitigate the electric field strength close to the HV electrode. The projection from end fitting is therefore selected as 62 cm. The electric field distribution with the optimized corona and grading rings is shown in Figure 43.

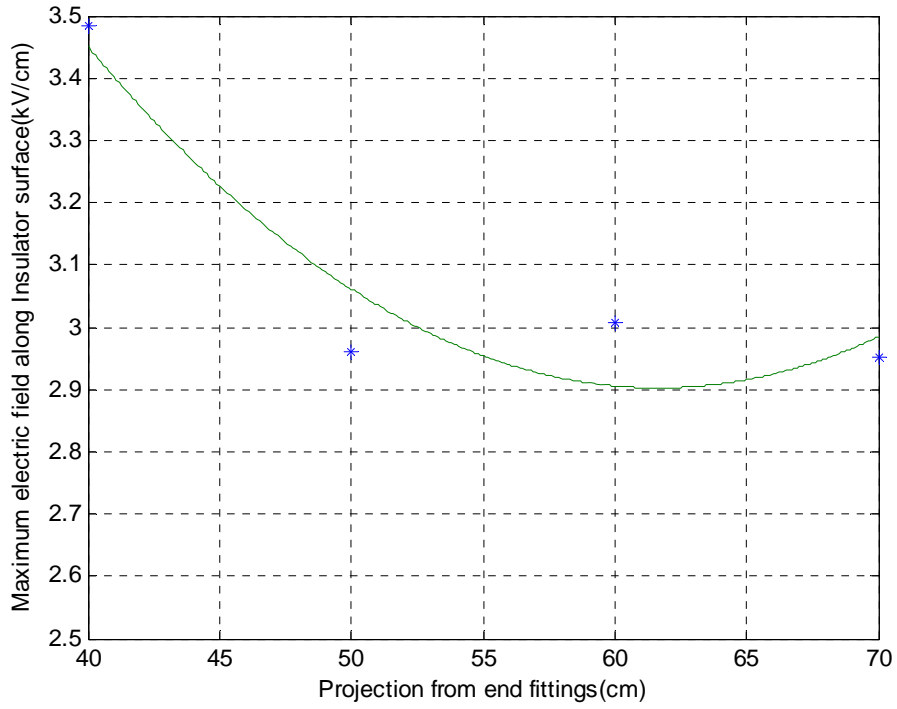


Figure 42. Maximum electric field as a function of projections from the end fitting

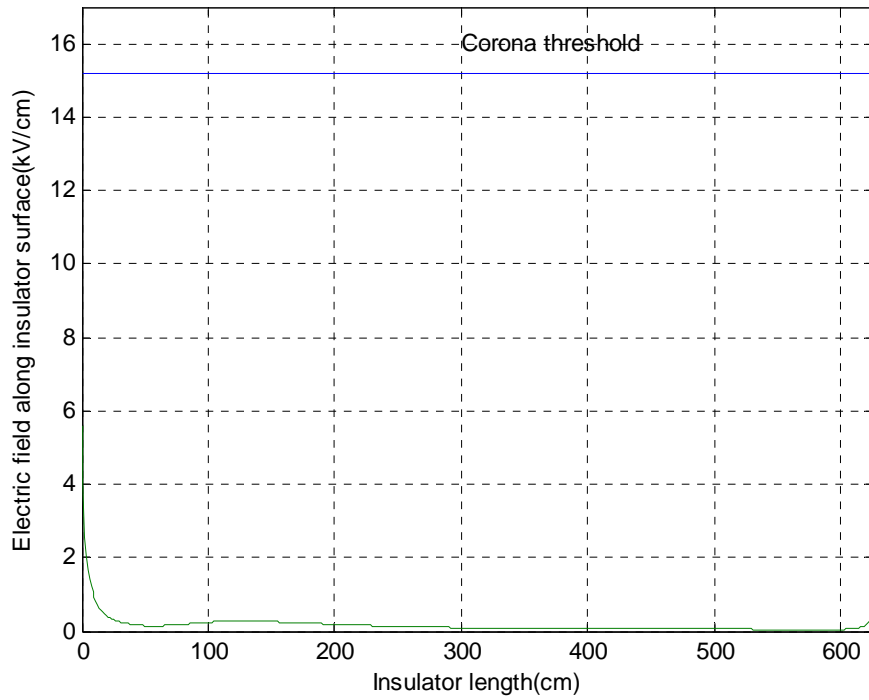


Figure 43. Electric field distribution along HVDC insulator surfaces with optimized corona and grading rings

### 6.3 Grading ring optimization under wet conditions

#### 6.3.1 Optimization for HVAC insulators

The optimizing process under dry conditions is repeated in this section to obtain the suitable dimensions of corona and grading rings under wet conditions. In Figure 44, the tube thickness and projection is fixed at 8 cm and 0 to build the function of maximum electric field strength versus ring radius. Meanwhile, In Figure 45, the grading ring radius and projection are set as constants of 70 cm and 0 cm, respectively, to determine the effect of the tube thickness. In Figure 46, the projection effect is measured with ring radius of 70 cm and tube thickness of 14 cm. In wet conditions, the results shows that ring radius, tube thickness, and projection all become major factors, to impact the field distribution, while in dry conditions, only the ring radius dominates.

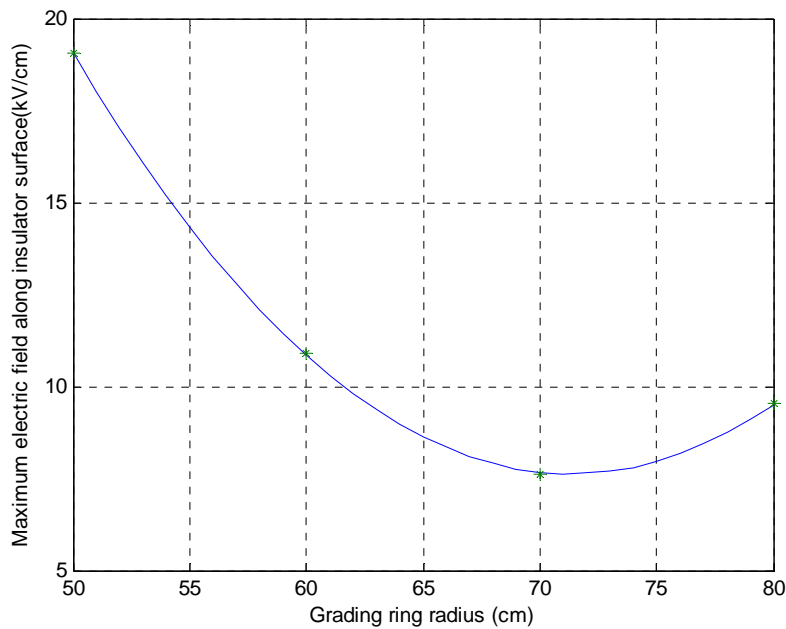


Figure 44. Maximum electric field as a function of ring radius of the HVAC insulator

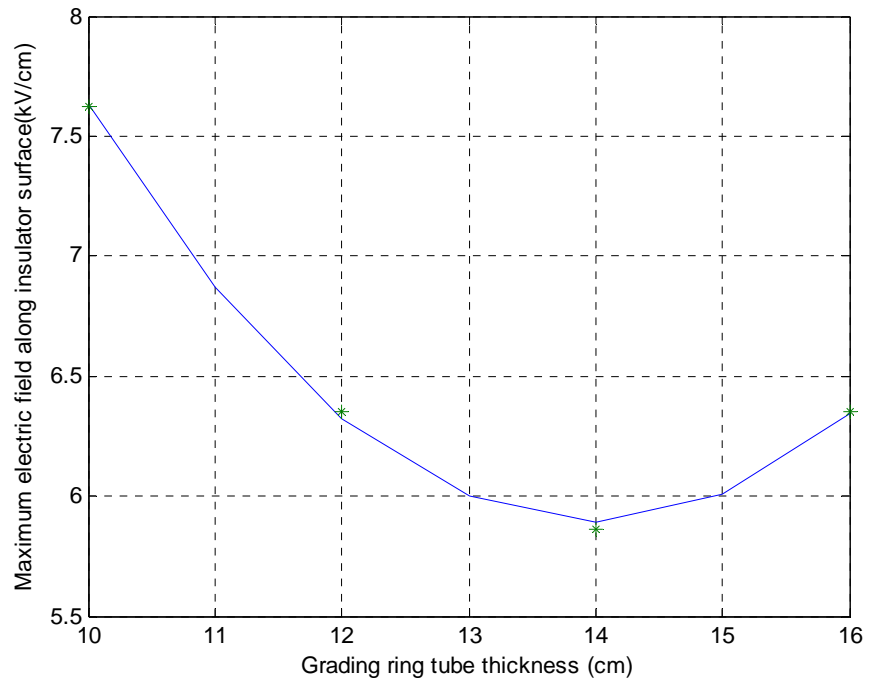


Figure 45. Maximum electric field as a function of ring tube thicknesses of the HVAC insulator

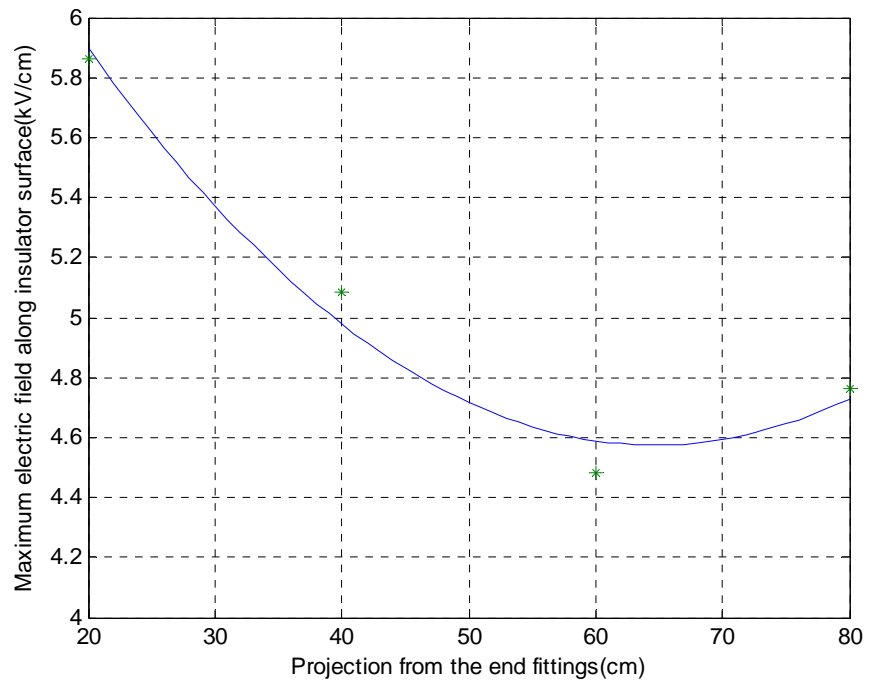


Figure 46. Maximum electric field as a function of projections from the end-fitting

The electric field distribution with the optimized corona rings and grading rings is shown in Figure 47. To make the plot clear, only 10% of insulator length close to electrode is shown. The maximum field strength is 3.65 kV/cm. The plot indicates that the electric field strength is significantly mitigated with optimized corona rings on the end-fittings of the insulator. It is shown that the grading rings, which have radius of 70 cm, tube thickness of 14 cm, and projection of 65 cm, have the best performance.

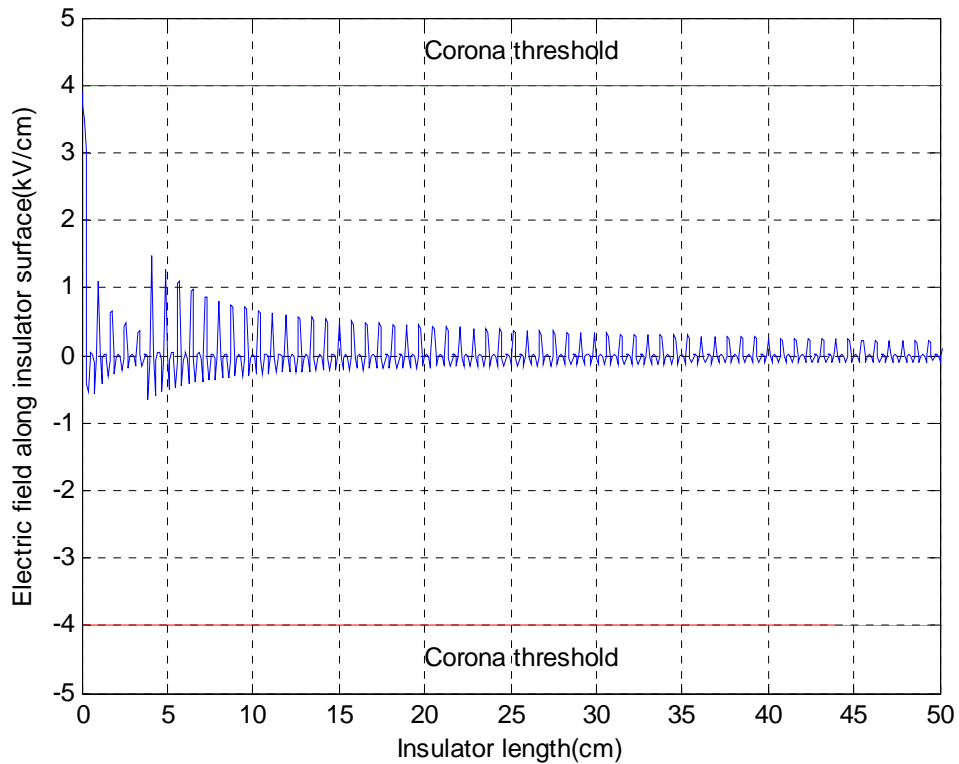


Figure 47. Electric field distribution of HVAC insulator surfaces with optimized corona and grading rings

### 6.3.2 Optimization for HVDC insulators

The dimensions of grading rings on HVDC insulators are optimized by the same method. Since the electric field strength with negative polarity is higher than that with positive polarity, the corona ring design is based on the negative polarity case.

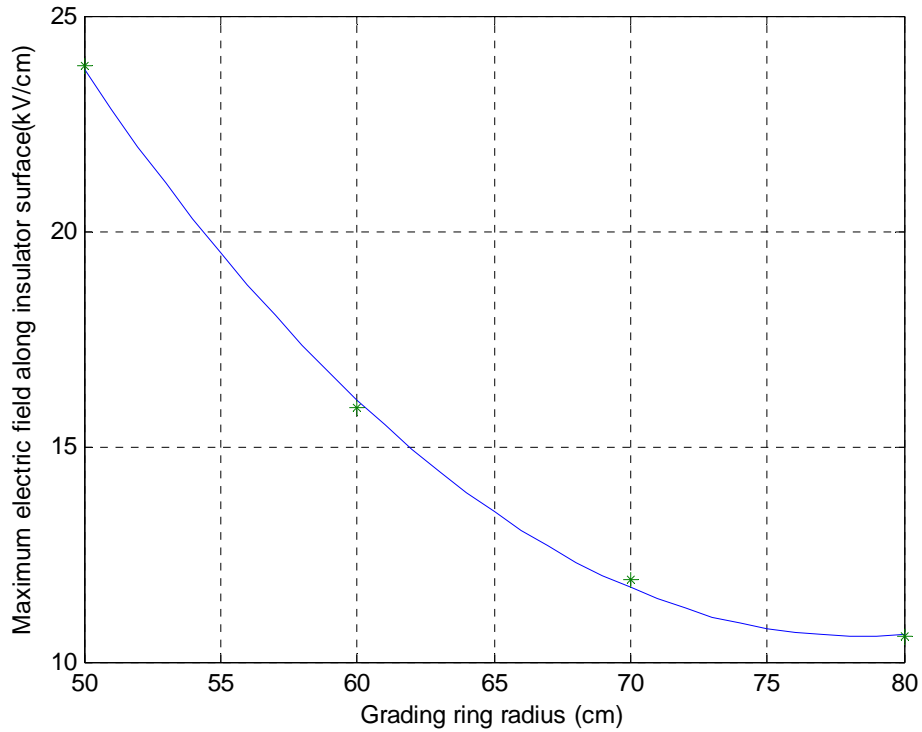


Figure 48. Maximum electric field as a function of radius of the HVDC insulator

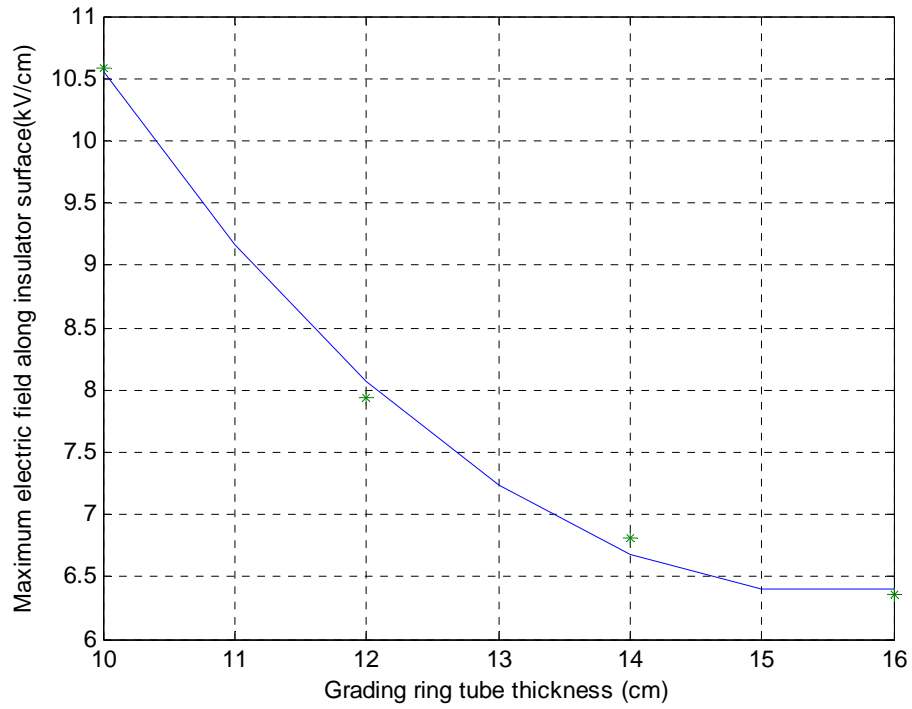


Figure 49. Maximum electric field as a function of tube thicknesses of the HVDC insulator

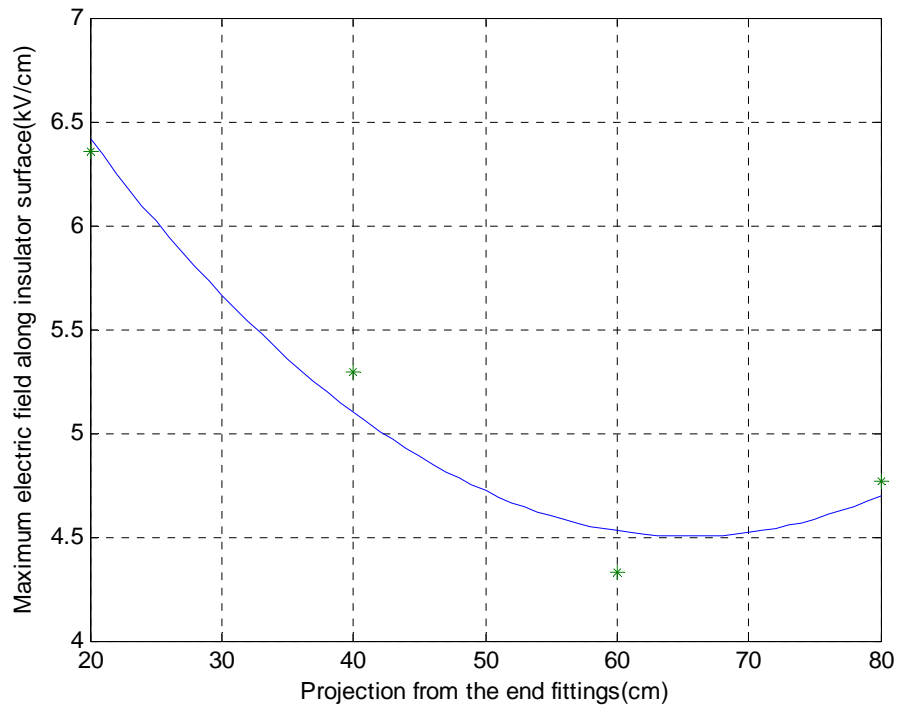


Figure 50. Maximum electric field as a function of projections of the HVDC insulator

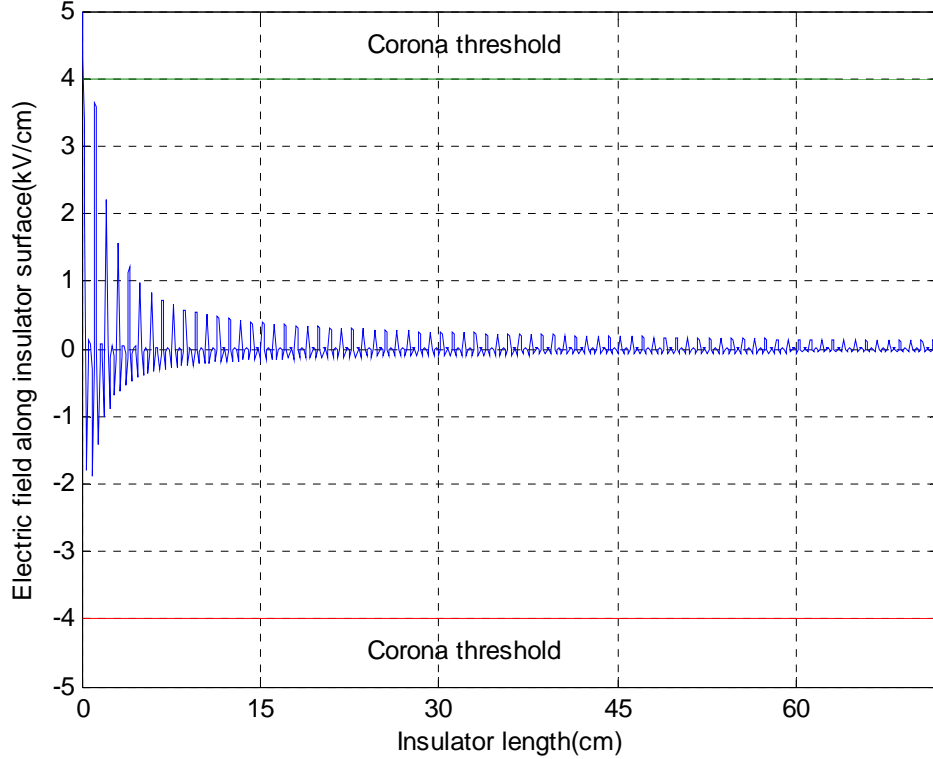


Figure 51. Electric field distribution of HVDC insulator surfaces with optimized corona and grading rings

Similarly, Figure 48 Figure 49 and Figure 50 show that the optimized grading rings have the radius of 80 cm, the tube thickness of 16 cm and the projection from end fitting of 68 cm. Figure 51 shows the electric field distribution of 10% of insulator length close to HV electrode with optimized grading rings. The maximum field strength is 3.93 kV/cm. It is concluded that with corona and grading rings, the electric field strength of the HVDC insulator is still more intensive than the field strength of the HVAC insulator.

## 7. CONCLUSIONS AND FUTURE WORK

### 7.1 Conclusions

This research focuses on the simulation of electric potential and field distribution on the HVDC composite insulators by using the charge simulation method. The fields of the conventional AC insulators are calculated to provide references for comparison. Both AC and DC insulators are simulated under dry and wet conditions. In the end, the dimensions of corona and grading rings are optimized. The conclusions of this project are shown below, all the conclusions are based on 500 kV AC and DC insulator models:

- (1) The electric field strength caused by water droplets rises with the decrease of separation between water droplets.
- (2) For DC lines, electric field distribution of negative polarity is higher than positive polarity in the part of the insulator close to the HV electrode.
- (3) Electric field on the insulator surface for DC lines is higher than field for AC lines at the part of the insulator close to HV electrode. Therefore, the ring radius and tube thickness of the dry HVDC insulator is 20.75% and 56.25% larger, when compared to HVAC insulator.
- (4) The electric field on the insulator surface under wet conditions is dramatically higher than field strength under dry conditions. Hence, the grading ring radius and tube thickness under wet conditions increase 25% and 28% for DC lines, respectively, when compared to the dry conditions. The projections from

end-fittings also need to be optimized in order to maintain the maximum electric field strength under corona threshold value.

## **7.2 Future works**

Future works will aim at the simulation of defects inside the insulator and further research of water droplets effects.

- (1) The properties of defects inside the insulators will be initially investigated. Then, the boundary conditions between defects and insulators will be found, based on Maxwell equations.
- (2) The electric field strength can affect the shape of water droplets and lead to droplet split. Meanwhile, the split of water droplets can also change the electric field distribution. In the end, the iteration process reaches a steady state, and the dynamic process needs to be analyzed.
- (3) The experiments will be conducted to verify the calculated results of the water droplets' case and the defects' case.

## REFERENCES

- [1] M. P. Bahrman, "HVDC transmission overview," *Transmission and Distribution Conference and Exposition, 2008. T&D. IEEE/PES*, pp. 1-7, 21-24 April 2008.
- [2] R. Lings, "Overview of transmission lines above 700 kV," *Power Engineering Society Inaugural Conference and Exposition in Africa, 2005 IEEE*, pp. 33-43, 11-15 July 2005.
- [3] R. S. Gorur, E. A. Cherney and J. T. Burnham, *Outdoor insulators*, Ravi S. Gorur Inc, 1999
- [4] P. B. Zhou, *Numerical analysis of electromagnetic fields*, Springer Verlag, 1993.
- [5] M. D. R. Beasley, J. H. Pickles, and G. Gallet, "Comparative study of three methods for computing electric fields," *Proceedings of the Institution of Electrical Engineers*, vol. 126, pp. 126-134, January 1979.
- [6] J. S. T. Looms, *Insulators with high voltages*, Peregrinus on behalf of the Institution of Electrical Engineers, 1988.
- [7] H. EI-Kishky and R. S. Gorur, "Electric potential and field computation along ac HV insulators," *IEEE Trans. Dielectrics and Electrical Insulation*, vol. 1, pp. 982-990, December 1994.
- [8] H. EI-Kishky and R. S. Gorur, "Electric field computation on an insulating surface with Discrete water droplets," *IEEE Trans. Dielectrics and Electrical Insulation*, vol. 3, pp. 450-456, June. 1996.
- [9] H. EI-Kishky and R. S. Gorur, "Electric field and energy computation on wet insulating surfaces," *IEEE Trans. Dielectrics and Electrical Insulation*, vol. 3, pp. 587-593, August. 1996.
- [10] H. singer, H. Steinbigler, and P. Weiss, "A charge simulation method for the calculation of high voltage fields," *IEEE Trans. Power Apparatus and Systems*, vol. PAS-93, pp. 1660-1668, September 1974.
- [11] N. H. Malik, "A review of the charge simulation method and its applications," *IEEE Trans. Electrical Insulation*, vol. 24, pp. 3-20, February 1989.

- [12] H. Tsuboi and T. Misaki, "The optimum design of electrode and insulator contours by nonlinear programming using the surface simulation method," *IEEE Trans. Magnetism*, vol. 24, pp. 35-38, January 1988.
- [13] T. Takuma, T. Kawamoto and H. Fujinami, "Charge simulation method with complex fictitious charges for calculating capacitive-resistive fields," *IEEE Trans. Power Apparatus and Systems*, vol. PAS-100, pp. 4665-4672, November. 1981.
- [14] S. S. Chowdhury, A. Lahiri and S. Chakravorti, " Surface resistance modified electric field computation in asymmetric configuration using surface charge simulation method: a new approach," *IEEE Trans. Dielectrics and Electrical Insulation*, vol. 19, pp. 1068-1075, June. 2012.
- [15] J. Phillips, D. J. Childs and H. M. Schneider, "Aging of Non-ceramic insulators due to corona from water drops," *IEEE Trans. Power Delivery*, vol. 14, pp. 1081-1089, July. 1999.
- [16] T. Doshi and R. S. Gorur, "Electric field computation of composite line insulators up to 1200 kV AC," *IEEE Trans. Dielectrics and Electrical Insulation*, vol. 18, pp. 861-867, June. 1996.
- [17] P. K. Mukherjee and C. K. Roy, "Computation of fields in and around insulators by fictitious points charges," *IEEE Trans. Electrical Insulation*, vol. EI-13, pp. 24-31, February 1978.
- [18] S. Schmidt, G. Zech and W. Otto, "E. Caredlli and L. Faina, "Open boundary, single-dielectric charge simulation method with the use of surface simulating charges," *IEEE Trans. Magnetism*, vol. 33, pp. 1192-1195, March 1997.
- [19] B. Lutz and J. Kindersberger, "Surface charge accumulation on cylindrical polymeric model insulators in air: simulation and measurement," *IEEE Trans. Dielectrics and Electrical Insulation*, vol. 18, pp. 2040-2048, December. 2011.
- [20] Skopec, J. G. Wankowicz and B. Sikorski, "Electric field calculation for an axially symmetric insulator with surface contamination," *IEEE Trans. Electrical insulation*, vol. 1, pp. 332-339, April 1994.
- [21] M. Abdel-Salam and E. K. Stanek, "Field optimization of high voltage insulators," *IEEE Trans. Industry Application*, vol. IA-22, pp. 594-601, July. 1986.

- [22] J. J. Lowke and F. D. Alessandro, "Onset corona fields and electrical breakdown criteria," *Journal of Physics D: Applied Physics*, vol. 36, pp. 2673-2682, October. 2003.
- [23] E. Kuffel and W. S. Zaengl, *High voltage engineering*, Pergamon Press, 1984
- [24] W. Que; S. A. Sebo., "Electric field and potential distributions along non-ceramic insulators with water droplets," *Electrical Insulation Conference and Electrical Manufacturing & Coil Winding Conference, 2001. Proceedings* , pp.441,444, 2001
- [25] Z. Guan, L. Wang; B. Yang, X. Liang; Z. Li, "Electric field analysis of water drop corona," *Power Delivery, IEEE Transactions on* , vol. 20, no. 2, pp. 964, 969, April 2005
- [26] H. Ootera and K. Nakanishi, "Analytical method for evaluating surface charge distribution on a dielectric from capacitive probe measurement-application to a cone-type spacer in  $\pm 500$  kV DC-GIS," *Power Delivery, IEEE Transactions on*, vol. 3, no. 1, pp. 165-172, January 1988.
- [27] W. Sima, F. P. Espino-Cortes, E. A. Cherney and S. H. Jayaram, , "Optimization of corona ring design for long-rod insulators using FEM based computational analysis," *Electrical Insulation, 2004. Conference Record of the 2004 IEEE International Symposium on*, pp. 480-483 September 2004.
- [28] G. Gerdin, V. Lakdawala and P. Basappa, "Computation of ac and dc electric field around a wet polluted insulator," *Electrical Insulation and Dielectric Phenomena, 2002 Annual Report Conference on*, pp. 176-179, 2002.
- [29] "IEEE Recommended Practice for Testing Insulation Resistance of Rotating Machinery," *IEEE Std 43-2000*, 2000.
- [30] G. Heger, H. J. Vermeulen, J. P. Holtzhausen and W. L. Vosloo, "A comparative study of insulator materials exposed to high voltage AC and DC surface discharges," *Dielectrics and Electrical Insulation, IEEE Transactions on*, vol. 17, no. 2, pp. 513-520, April 2010.

- [31] S. Kumara, I. R. Hoque, S. Alam, Y. V. Serdyuk and S. M. Gubanski, "Surface charges on cylindrical polymeric insulators," *Dielectrics and Electrical Insulation, IEEE Transactions on*, vol. 19, no. 3, pp. 1076-1083, June 2012.